bioRxiv preprint doi: https://doi.org/10.1101/2020.03.02.973685; this version posted October 14, 2021. The copyright holder for this preprint (which was not certified by peer review) is the author/funder. All rights reserved. No reuse allowed without permission.

Chromatin remodelling by INO80 at promoter proximal pause sites promotes premature termination of mRNA synthesis

Sara Luzzi[1,*], Ugo Szachnowski[2,*], Sarah Greener[1], Kenny Schumacher[3,4,5,6], Stuart Fulton[7], Camille Gautier[2], Kang Hoo Han[8], Jack Darke[1], Rossana Piccinno[9], Anne Lafon[2,9], B. Franklin Pugh[8,10], Didier Devys[3,4,5,6], Laszlo Tora[3,4,5,6], Antonin Morillon[2†], and Manolis Papamichos-Chronakis[4,11†]

Affiliations:

[1]Biosciences Institute, Faculty of Medical Sciences, Newcastle University, Newcastle upon Tyne, NE2 4HH, United Kingdom

[2]ncRNA, Epigenetic, and Genome Fluidity, Institut Curie, PSL Research University, CNRS UMR 3244, Pierre et Marie Curie University, 26 rue d'Ulm, 75248 Paris Cedex 05, France

[3]Institut de Génétique et de Biologie Moléculaire et Cellulaire, 67404, Illkirch, France

[4]Centre National de la Recherche Scientifique, UMR7104, 67404, Illkirch, France

[5]Institut National de la Santé et de la Recherche Médicale, U964, 67404, Illkirch, France

[6]Université de Strasbourg, 67404, Illkirch, France

[7]Department of Molecular Physiology and Cell Signaling, Institute of Systems, Molecular, and Integrative Biology, University of Liverpool, Liverpool L69 7ZB, UK

[8]Center for Eukaryotic Gene Regulation, Department of Biochemistry and Molecular Biology, The Pennsylvania State University, University Park, PA 16802, USA

[9]Institut Curie, PSL Research University, CNRS, UMR3664, 26 rue d'Ulm, 75248 Paris, France

bioRxiv preprint doi: https://doi.org/10.1101/2020.03.02.973685; this version posted October 14, 2021. The copyright holder for this preprint (which was not certified by peer review) is the author/funder. All rights reserved. No reuse allowed without permission.

[10]Department of Molecular Biology and Genetics, Cornell University, Ithaca, NY 14853, USA

[11]Lead Contact

*These authors contributed equally to this work

†Correspondence to: antonin.morillon@curie.fr and manolis.papamichos@newcastle.ac.uk

bioRxiv preprint doi: https://doi.org/10.1101/2020.03.02.973685; this version posted October 14, 2021. The copyright holder for this preprint (which was not certified by peer review) is the author/funder. All rights reserved. No reuse allowed without permission.

Abstract

How co-transcriptional RNA quality control is regulated remains poorly understood. Here, we report that in *S. cerevisiae* premature transcription termination of mRNAs is regulated by the evolutionarily conserved ATP-dependent chromatin remodeling INO80 complex. Loss of INO80 leads to an increase in promoter-proximally paused RNA Polymerase II and defective progression into the gene body. We show that promoter-proximal transcriptional pausing correlates with loading of RNA surveillance and transcription termination factors to mRNA transcripts. Cells lacking INO80 are defective for the Nrd1-Nab3-Sen1 (NNS)-dependent pathway for transcription termination at snRNA genes and promoter-proximally sites of mRNA genes. We demonstrate that INO80 promotes the association of the RNA surveillance and termination factor Nab2 with short promoter-proximal mRNA transcripts. We provide evidence that co-transcriptional recruitment of Nab2 to chromatin is regulated by INO80, which enables the interaction of Nab2 with the histone variant H2A.Z. Our work suggests a chromatin mechanism for premature transcription termination at promoter-proximally pausing sites, linking RNA quality control to the transcriptional process.

bioRxiv preprint doi: https://doi.org/10.1101/2020.03.02.973685; this version posted October 14, 2021. The copyright holder for this preprint (which was not certified by peer review) is the author/funder. All rights reserved. No reuse allowed without permission.

INTRODUCTION

Elimination of aberrant mRNAs is essential for proper gene expression. In eukaryotic cells nuclear RNA surveillance and quality control mechanisms monitor mRNA biogenesis co-transcriptionally and terminate transcription prematurely for degradation of the nascent RNA transcript[1]. Elegant genome-wide studies in the budding yeast *Saccharomyces cerevisiae* have suggested that unproductive transcriptional elongation of protein coding genes is wide-spread and common[2,3]. Furthermore, promoter-proximal short mRNAs enriched in 3'-oligo(A) tails have been identified[4], indicating extensive premature termination across the yeast protein-coding genome[5]. Likewise, only 10% of promoter-proximally paused polymerases was shown to enter productive elongation in human cells, with the remaining being prematurely terminated during abortive elongation[6,7].

The major nuclear RNA quality control pathway in yeast is mediated by the RNA surveillance complex Nrd1-Nab3-Sen1 (NNS)[8] and the Rrp6-dependent nuclear exosome complex with 3' exonuclease activity[9]. The NNS-dependent nuclear RNA quality control pathway acts prominently to restrict the extensive and pervasive transcription of non-coding RNAs (ncRNAs)[10]. Nrd1 and Nab3 have also been found to be recruited at active protein-coding genes with a preference near their 5' end and bind most mRNA transcripts[11-15], suggesting a genome-wide role for NNS in mRNA transcription termination[15] and co-transcriptional control of mRNA metabolism. However, this model has been challenged by a separate study, which proposed that only a few mRNA genes are subject to transcriptional attenuation by the NNS complex[16]. Thus, although the RNA surveillance and termination pathways have been characterized in molecular detail, the mechanisms regulating premature transcription termination during mRNA synthesis by Pol II remain unclear.

In metazoans, short, promoter-associated polyadenylated mRNA transcripts[17] have been found to associate with Pol II pausing[18], with premature termination and exosome-dependent

bioRxiv preprint doi: https://doi.org/10.1101/2020.03.02.973685; this version posted October 14, 2021. The copyright holder for this preprint (which was not certified by peer review) is the author/funder. All rights reserved. No reuse allowed without permission.

degradation coinciding with promoter-proximal pausing sites[19]. Experiments with chemical transcriptional inhibitors indicated high rates of turnover and premature termination of promoter-proximal paused Pol II[6,20,21], suggesting regulation of gene expression by transcriptional attenuation. Even though promoter-proximal pausing plays an important regulatory role in eukaryotic transcription[22-25], how pausing is linked to premature termination remains poorly understood.

Eukaryotic transcription is controlled by the underlying chromatin structure. ATP-dependent chromatin remodelling enzymes shape the chromatin landscape and act at almost all stages of RNA production controlling transcription activation and silencing, modulation of transcriptional rates, transcription termination and RNA export from the nucleus[26-30]. In mammals, premature termination of mRNA genes and promoter-proximal transcriptional pausing have been associated with nucleosome organization[19]. However, the role of chromatin remodelers in co-transcriptional RNA quality control remains elusive.

The multisubunit ATP-dependent chromatin remodelling complex INO80 has a well-established and important role in transcription across eukaryotes[31]. INO80 is enriched at the transcription start sites (TSS) of most active and poised mRNA genes in yeast and mammals[32,33]. The nucleosome remodelling activity of INO80 is important for the exchange of the histone variant H2A.Z for H2A in nucleosomes and for controlling nucleosome positions[31]. While it is generally proposed that the function of INO80 during transcription is to control transcription initiation, INO80 physically interacts with the elongating RNA Polymerase II machinery[34,35] and binds to mRNAs[36,37]. This indicates a -yet- undefined role for INO80 in the transcriptional process.

Here we investigate the role of INO80 in transcription regulation in *S. cerevisiae*. Using Native Elongating Transcript sequencing (NET-seq) we analyse how the process of transcription is regulated by INO80 at nucleotide resolution. We show that INO80 enables

bioRxiv preprint doi: https://doi.org/10.1101/2020.03.02.973685; this version posted October 14, 2021. The copyright holder for this preprint (which was not certified by peer review) is the author/funder. All rights reserved. No reuse allowed without permission.

the progression of Pol II from the promoter-proximal region into the gene body. Our analysis indicates that promoter-proximal pausing of Pol II is linked to loading of transcription termination and RNA processing factors to mRNA transcripts. Mechanistically our study reveals that INO80 modulates the interaction between the RNA surveillance and termination factor Nab2 and H2A.Z, enabling recruitment of Nab2 to chromatin. Overall, our results suggest that the chromatin remodelling function of INO80 promotes premature transcription termination.

bioRxiv preprint doi: https://doi.org/10.1101/2020.03.02.973685; this version posted October 14, 2021. The copyright holder for this preprint (which was not certified by peer review) is the author/funder. All rights reserved. No reuse allowed without permission.

RESULTS

Defective progression of Pol II from the promoter proximal region into the gene body in the absence of INO80

To illuminate the role of INO80 in transcription, we performed Native Elongating Transcript NET-seq analysis in Wild-Type (WT) and *ino80Δ* yeast cells expressing a FLAG-tag version of the largest subunit of the RNA Polymerase II complex, Rpb1 (Extended Data Fig. 1a, b). NET-seq captures nascent RNAs bound to transcriptionally engaged Pol II and sequences the 3'-end of the purified RNAs, thus providing a detailed map of elongating Pol II across the genome at nucleotide resolution[38]. Therefore, and to avoid confusion with the term "nascent RNAs" that is commonly used to describe newly synthesized RNAs that are not necessarily associated with Pol II[39], we will henceforth refer to the Pol II-associated transcripts captured by NET-seq as Pol II density.

Following removal of duplicated reads and DEseq normalization, NET-seq densities were computed as normalized counts over gene length and their distribution across the gene was compared between the two strains. Consistent with previous reports[38,40], promoter-proximal region showed sense Pol II density, with a subsequent reduction further into the gene body in WT cells **(**Fig. 1a). Interestingly, in *ino80Δ* cells, while sense Pol II density was reduced at the promoter-proximal peak, it decreased further downstream the promoter-proximal region, compared to WT (Fig 1a). Changes in the abundance of sense and antisense NET-seq reads at mRNA genes in *ino80Δ* did not correlate (Extended Data Fig. 1c, r=0.04), indicating that altered sense Pol II density in the absence of INO80 is independent of antisense transcription.

We explored whether the decrease in Pol II density downstream the promoter proximal region in *ino80Δ* indicates defective progression of RNA Polymerase II into the gene body. To test this possibility, we calculated Traveling Ratio (TR) values for all mRNA genes by

bioRxiv preprint doi: https://doi.org/10.1101/2020.03.02.973685; this version posted October 14, 2021. The copyright holder for this preprint (which was not certified by peer review) is the author/funder. All rights reserved. No reuse allowed without permission.

125 comparing the Pol II density in the gene body relative to the promoter-proximal region of the
126 first 200bp after the TSS (Fig. 1b). In WT cells, 68% of protein-coding genes exhibited
127 higher Pol II density at the promoter-proximal region compared to Pol II density in the gene
128 body for (TR<1), indicating accumulation of Pol II proximally to promoter for most of the
129 genes. Loss of INO80 led to an overall significant reduction in TR, with 809 genes exhibiting
130 a decrease in TR of at least 1.5 fold-change compared to WT (Fig. 1b). Overall, 73% of genes
131 demonstrated a TR<1 in *ino80Δ*. This indicates a genome-wide defect in progression of Pol II
132 from the promoter-proximal region into the gene body in the absence of INO80.

133 INO80 physically interacts with the elongating RNA Polymerase II complex[34,35] and is
134 enriched within gene bodies[33,41]. To evaluate its role during transcription elongation, we
135 asked whether the enrichment of INO80 inside gene bodies correlates with the intragenic
136 levels of Pol II. ChIP-exo analysis provides near single-nucleotide resolution of factor
137 binding to DNA[42] and can distinguish between recruitment inside and outside the gene body
138 with great accuracy. When the Ino80[41] and Rpb1 ChIP-exo densities within the gene bodies
139 were compared, a strong, positive correlation between their enrichment was observed (Fig.
140 1c, r=0.68). This indicates that the presence of INO80 inside the gene is associated with
141 transcription elongation activity.

142 Chromatin remodelling activity and functionality of the INO80 complex relies on the INO80-
143 specific subunits Arp5 and Arp8[31]. Cells lacking either *INO80* or the INO80-specific subunits
144 *ARP5* or *ARP8* grew poorly in the presence of 6-azauracil (6-AU) (Fig. 1d and Extended
145 Data Fig. 1d, e), an inhibitor of GTP biosynthesis which sensitizes transcriptional elongation
146 mutants[43]. Therefore, these results suggest that INO80 promotes transcription elongation,
147 supporting a genome-wide, post-initiation role for INO80 in gene expression.

148 **Global downregulation of Pol II transcription in the absence of INO80 is associated**
149 **with defective mRNA degradation**

bioRxiv preprint doi: https://doi.org/10.1101/2020.03.02.973685; this version posted October 14, 2021. The copyright holder for this preprint (which was not certified by peer review) is the author/funder. All rights reserved. No reuse allowed without permission.

Increase in transcription initiation can lead to enhanced pausing of Pol II at predetermined sites[44]. We therefore asked whether transcription rates are increased in the absence of INO80, by comparing the levels of newly synthesized mRNAs in WT and *ino80Δ* cells. Cells grown in rich medium were pulse-labelled with 4-thiouracil (4tU) and mixed in a fixed ratio with labelled *S.pombe* cells (spike-in) for normalization[45]. In parallel, 4tU labelling was also conducted in *ino80Δ* cells expressing wild-type *INO80* from a plasmid, serving as a control for *ino80Δ*-mediated changes in RNA expression. Purified total (steady state) and labelled (newly synthesized) RNA from all samples were subjected to sequencing.

After normalization to the *S. pombe* spiked-in signal and applying a cutoff of 1.5-fold change and p-value < 0.05, only 3.6% of all protein coding genes showed significant increase in newly synthesized mRNA levels in *ino80Δ* (n=178, Fig. 3a). Contrary, 34% of the protein-coding genome demonstrated a significant reduction in mRNA synthesis in *ino80Δ* compared to WT (n=1706, Fig. 3a). The downregulation of mRNA synthesis rates was INO80-dependent, since in *ino80Δ* cells expressing *INO80* from an episomal plasmid, less than 4% of genes had markedly decreased newly synthesized mRNA levels (n=193, Extended Data Fig. 3a). Therefore, deletion of INO80 induces genome-wide downregulation of mRNA synthesis rates, arguing against increased transcription initiation as the underlying cause of enhanced Pol II pausing in *ino80Δ*.

Interestingly, despite the global decrease in newly synthesized mRNA levels in *ino80Δ*, the cellular, total mRNA levels for 81% of the protein-coding genes did not significantly change, while 13% were increased in the absence of INO80 (Fig. 3b). This disentanglement between newly synthesized and total RNAs suggests buffering of mRNA transcript levels[46] in *ino80Δ* by a compensatory mechanism. Cellular mRNA levels are determined by the rates of mRNA synthesis and degradation. To understand why cellular mRNA levels remain high in *ino80Δ*, we conducted comparative dynamic transcriptome analysis (cDTA)[47], which measures

bioRxiv preprint doi: https://doi.org/10.1101/2020.03.02.973685; this version posted October 14, 2021. The copyright holder for this preprint (which was not certified by peer review) is the author/funder. All rights reserved. No reuse allowed without permission.

mRNA synthesis and decay rates (SR and DR respectively) for all protein-coding genes. Comparison of the SR and DR changes in *ino80Δ* relative to WT revealed that the decrease in SR observed in *ino80Δ* positively correlated with a concomitant decrease in DR (r=0.47, p-value=$2.9e^{-233}$, Fig 3c). This indicates that the defect in Pol II transcription in *ino80Δ* is associated with compromised mRNA degradation, in a similar fashion to what has been observed for the rpb1-N488D mutant[47], which reduces the processivity of Pol II[48].

To verify that mRNAs are stabilized in the absence of INO80, we analysed mRNA decay rates following transcription inhibition with thiolutin in WT and ino80Δ cells. Thiolutin was used at concentration below the threshold reported to affect mRNA half-life[49] and mRNA values were normalized relative to the stable scR1 RNA, which is transcribed by Pol III. The relative abundance of *NRD1*, *RNA1* and *HPT1* transcripts, which showed decreased DR in the cDTA analysis (Extended data Fig. 3b), was markedly higher in *ino80Δ* compared to WT after transcription inhibition (Fig. 3d and Extended data Fig. 3c). Therefore, the concomitant change in mRNA synthesis and degradation in *ino80Δ* suggest that the transcriptional role of INO80 is linked to RNA decay by buffering steady state mRNA levels.

Promoter-proximal Pol II pausing is linked to increased loading of RNA surveillance and termination factors to mRNA transcripts

The results from our NET-seq and 4tU-seq analysis prompted us to evaluate whether promoter-proximal pausing is linked to nuclear RNA quality control and premature transcription termination.

The nuclear RNA cleavage and termination factor Nab2[50] and the Trf4/Trf5-Air1/Air2-Mtr4 polyadenylation (TRAMP) complex are required for processing and delivering nascent transcripts to the nuclear exosome for degradation[51-55]. Nab2, Mtr4 and the Nab3 subunit of the NNS complex bind most of mRNAs[4,56]. We retrieved published genomic data for RNA

bioRxiv preprint doi: https://doi.org/10.1101/2020.03.02.973685; this version posted October 14, 2021. The copyright holder for this preprint (which was not certified by peer review) is the author/funder. All rights reserved. No reuse allowed without permission.

199 binding (CRAC) for Nab3, Nab2 and Mtr4[4,56]. and corrected their binding to mRNA
200 transcripts for their respective gene transcription levels as measured by CRAC-Rpb1[56] (Fig.
201 4a). This normalisation generated an index of Transcript Instability (TI) values for all
202 protein-coding genes, allowing us to quantitatively assess the level of premature transcription
203 termination taking place within each mRNA gene.

204 We evaluated whether accumulation of Pol II at the promoter-proximal region is associated
205 with premature termination. TI values were calculated for the promoter-proximal region (TSS
206 to TSS+200) and the downstream gene body (TSS+200 to PAS). Genes were clustered in
207 four groups based on their TR values in WT conditions (Fig. 4b) and $TIs^{Mtr4/Nab3/Nab2}$ were
208 analysed for the genes of each group. Intriguingly, a reciprocal relationship between TR and
209 promoter-proximal TI was observed: genes with increased accumulation of Pol II at the
210 promoter-proximal region relative to the gene body (low TR) had high $TI^{Mtr4/Nab3/Nab2}$, while
211 genes with little or no promoter-proximal accumulation of Pol II (high TR) had low TI (Fig.
212 4c). Contrary, no decrease in the $TI^{Mtr4/Nab3/Nab2}$ values was observed within the gene body in
213 the four TR groups (Fig. 4c). Therefore, defective progression of Pol II from the promoter-
214 proximal region correlates with early transcription termination at the same region.

215 **Functional and physical interactions link INO80 to RNA quality control and NNS-**
216 **dependent transcription termination pathway**

217 Since in *ino80Δ* cells Pol II is stalled at genomic sites associated with increased binding of
218 RNA surveillance factors to RNA, we interrogated whether the role of INO80 in gene
219 expression is functionally linked to the RNA quality control process. Abd1 is an essential
220 m7G cap methyltransferase that prevents mRNA destabilization and degradation[57]. Deletion
221 of *ARP8* in the *abd1-DAmP* strain, which expresses a hypomorphic allele of *ABD1*[58], led to
222 synthetic lethality in non-permissive conditions (Fig. 5a), suggesting that INO80 is essential
223 for cellular viability when mRNAs are destabilized. Deletion of *ARP8* in the *nrd1-V368G*

bioRxiv preprint doi: https://doi.org/10.1101/2020.03.02.973685; this version posted October 14, 2021. The copyright holder for this preprint (which was not certified by peer review) is the author/funder. All rights reserved. No reuse allowed without permission.

(designated as *nrd1-5*) mutant strain, which is deficient in transcription termination[8] led to synthetic lethality in 6-AU (Fig. 5b). In addition, the *arp8Δ* and *nrd1-5* mutants were epistatic for *INO1* expression (Fig. 5c) suggesting that the INO80 and NNS complexes work in the same pathway in gene regulation. These genetic interactions link INO80 to co-transcriptional RNA quality control, prompting us to test whether the INO80 complex physically associates with the transcription termination machinery.

Protein co-immunoprecipitation analysis after nucleic acid removal demonstrated that the INO80 complex physically interacts with both Nrd1 and Nab2 *in vivo* (Fig. 5d, e). Contrary, we could not detect a physical interaction between the INO80 complex and the component of cleavage and polyadenylation factor IA (CF IA) complex Pcf11 (Extended Data Fig. 4a), which promotes transcription termination at the PAS.

INO80 promotes NNS-dependent transcription termination

To explore the possibility that INO80 is involved in Nrd1-dependent termination, we employed the well-characterized *ACT-SNR^{TTS}-CUP* reporter system[8,59] (Extended Data Fig. 5a). Briefly, cells were transformed with ACT-CUP plasmids without or with the Transcription Termination Site (TTS) of the snoRNA gene *SNR13* (*SNR^{TTS}*) inserted prior to the CUP1 gene, which confers resistance to copper. Termination of snoRNAs, including *SNR13,* is regulated by the NNS complex[8,60]. INO80 is co-enriched with Nrd1 at the endogenous *SNR13*^{TTS} region (Extended Data Fig. 4b), making the *ACT-SNR^{TTS}-CUP* reporter a suitable system to test the role of INO80 in NNS-dependent transcription termination. Contrary to WT, *ino80Δ* cells transformed with the *ACT-SNR^{TTS}-CUP* plasmid were able to grow in the presence of copper, suggesting read-through transcription of *CUP1* (Fig. 6a). RT-qPCR analysis using primer pairs that target the regions before and after the *SNR13^{TTS}* insertion site in the reporter plasmids showed a significant increase in the relative transcription of *CUP1* in the *ACT-SNR^{TTS}-CUP* plasmid in *ino80Δ* and *arp8Δ* mutants by 2.8-

bioRxiv preprint doi: https://doi.org/10.1101/2020.03.02.973685; this version posted October 14, 2021. The copyright holder for this preprint (which was not certified by peer review) is the author/funder. All rights reserved. No reuse allowed without permission.

249 fold and 3.5-fold respectively (Fig. 6b and Extended Data Fig. 5c). Similarly, a 3-fold
250 increase was observed in *nrd1-5* cells, in accordance to previous studies[8] (Fig. 6b and
251 Extended Data Fig. 5c). Inducible degradation of Ino80 also resulted in an acute increase in
252 relative *CUP1* levels from the *ACT-SNR*^{TTS}*-CUP* but not from the control *ACT-CUP* plasmid
253 lacking the transcription termination site (Extended Data Fig. 5d). Deletion of either *INO80*
254 or *ARP8* did not significantly alter gene expression of any of the known transcription
255 termination and RNA surveillance factors (Extended Data Table 2). These results support a
256 direct role for INO80 in transcription termination at the *SNR13*^{TTS} termination site.

257 To further substantiate a role for INO80 in NNS-dependent termination, we evaluated read-
258 through transcription at the termination sites of endogenous snoRNA genes. Using paired-
259 end, spiked-in RNA sequencing we mapped the sense RNA-seq reads encompassing the TTS
260 of the snoRNA genes in WT and *ino80Δ*. In the absence of INO80 read-through transcripts
261 are significantly increased for the majority of the snoRNA genes, but not for the ribosomal
262 protein coding gene *YNL096C* (Fig. 6c, d, and Extended Data Fig. 5e and Extended Data
263 Table 3). The increase in readthrough transcripts in *ino80Δ* is not due to defective
264 degradation, as termination of snoRNAs in cells deleted for the 5'-3' exoribonuclease *XRN1*
265 was normal, while deletion of the nuclear exosome subunit *RRP6* compromised termination
266 only at a small number of specific snoRNA genes, in accordance with previous studies[61,62]
267 (Fig. 6d and Extended Data Table 2). These results suggest that INO80 promotes NNS-
268 dependent transcription termination.

269 To investigate the effect of INO80 loss on premature termination of mRNA synthesis, we
270 focused our analysis on the *NRD1* gene, which is a known target for promoter-proximal
271 transcription termination by the NNS/Rrp6 pathway[8,61]. Ino80 is enriched at the promoter-
272 proximal region of *NRD1* (Extended Data Fig. 5f) and loss of INO80 resulted in increased
273 promoter-proximal Pol II density at *NRD1* compared to WT (Extended Data Fig. 5g). To

bioRxiv preprint doi: https://doi.org/10.1101/2020.03.02.973685; this version posted October 14, 2021. The copyright holder for this preprint (which was not certified by peer review) is the author/funder. All rights reserved. No reuse allowed without permission.

assess termination proximally to promoters and at the end of the gene we conducted quantitative 3' rapid amplification of cDNA ends (3' RACE) using gene-specific primers for either the promoter-proximal or the PAS region of the *NRD1* gene respectively. Deletion of *RRP6* increased the relative abundance of promoter-proximally terminated *NRD1* mRNAs compared to WT, while also upregulated the expression of *NRD1* transcripts terminated at the end of the gene, in line with RNA-seq data (Fig. 6e and Extended Data Fig. 5h). Notably, deletion of either *INO80* or *APR8* attenuated the expression of early terminated transcripts compared to the PAS-terminated *NRD1* transcripts (Fig. 6e). This suggests that the INO80 complex promotes premature transcription termination at mRNA genes.

INO80 promotes chromatin recruitment and association of Nab2 with H2A.Z

To understand the mechanism underlying the function of INO80 in premature termination, we hypothesized that INO80 regulates the recruitment of the RNA quality control machinery to chromatin. The RNA surveillance factor Nab2 promotes transcription termination[50]. Nab2 binds promoter-proximal mRNAs that are prematurely terminated[4], including *NRD1* (Extended Data Fig. 6a), while it is co-transcriptionally recruited to the gene body of actively transcribed mRNA genes[12]. We therefore tested by ChIP-qPCR whether association of Nab2 with chromatin depends on INO80. Co-transcriptional recruitment of Nab2 to the promoter-proximal region of *NRD1* was reduced in the absence of INO80 (Fig. 7a and Extended Data Fig. 6b). Likewise, Nab2 co-transcriptional recruitment at the *SNR13* gene was also compromised in *ino80Δ* (Extended Data Fig. 6c). Co-immunoprecipitation for Nab2 confirmed that the physical interaction between Nab2 and Rpb1 was independent of INO80 (Extended Data Fig. 6d), excluding the possibility that the decreased recruitment of Nab2 to chromatin is caused by compromised binding to the Pol II machinery. To evaluate whether loss of INO80 disrupts the association of Nab2 with the promoter-proximal *NRD1* transcript, we conducted quantitative RNA-IP for Nab2. In *ino80Δ* cells the binding of Nab2 to

bioRxiv preprint doi: https://doi.org/10.1101/2020.03.02.973685; this version posted October 14, 2021. The copyright holder for this preprint (which was not certified by peer review) is the author/funder. All rights reserved. No reuse allowed without permission.

promoter-proximal *NRD1* RNA was significantly reduced compared to its binding to the PAS-proximal *NRD1* region (*3'-NRD1*) (Fig. 7b). These results suggest that INO80 regulates recruitment of Nab2 to chromatin to promote its binding to nascent RNAs.

We sought to gain insight into how INO80 promotes recruitment of Nab2 to chromatin. Promoter-proximal nucleosomes are enriched in the histone variant H2A.Z[63]. H2A.Z has been suggested to have a role in RNA quality control and non-PAS transcription termination in *D.melanogaster* and *S.pombe*[64-66]. INO80 preferentially remodels nucleosomes containing H2A.Z and controls the dynamic association of H2A.Z with chromatin[33,67-69], raising the possibility that H2A.Z might be involved in NNS-dependent termination. Cells lacking *HTZ1*, which encodes for H2A.Z in budding yeast, grew in the presence of copper when transformed with the *ACT-SNR*^{TTS}*-CUP* plasmid (Fig.7c and Extended Data Fig. 6f), suggesting that H2A.Z suppresses read-through transcription from NNS-dependent termination sites. Promoter-proximally terminated *NRD1* transcripts were decreased in *htz1Δ* compared to WT (Fig. 7d), indicating that loss of H2A.Z compromises premature transcription termination of mRNA genes. In line with defective early termination, co-transcriptional recruitment of Nab2 at the promoter-proximal region of *NRD1* was reduced in *htz1Δ* cells (Fig. 7e and Extended Data Fig. 6g). Co-immunoprecipitation assays after nucleic acid removal demonstrated that H2A.Z interacts with Nab2, even after non-physiological high-salt wash conditions, but not with Pcf11 (Fig. 7f and Extended Data Fig. 7h, i). Since our evidence indicate that H2A.Z is involved in premature transcription termination and RNA quality control at mRNA genes, we asked whether INO80 controls the interaction between H2A.Z and Nab2. Remarkably, binding of Nab2 to H2A.Z was decreased in *ino80Δ* (Fig. 7f). This suggests that INO80 enables the recruitment of the Nab2 RNA surveillance machinery to chromatin by promoting its interaction with H2A.Z.

bioRxiv preprint doi: https://doi.org/10.1101/2020.03.02.973685; this version posted October 14, 2021. The copyright holder for this preprint (which was not certified by peer review) is the author/funder. All rights reserved. No reuse allowed without permission.

DISCUSSION

Here, we elucidate a role for INO80 in transcription. We report that INO80 enables recruitment of the RNA quality control machinery to transcribed mRNA genes for early transcription termination, promoting transcription elongation. Our data suggest that by removal of Pol II and termination of unproductive transcription, INO80 defines a chromatin-based pathway for co-transcriptional mRNA quality control. Based on our results we propose that control of premature transcriptional termination by INO80-dependent chromatin remodelling is a genome-wide regulatory mechanism of eukaryotic gene expression.

Linking mRNA quality control to chromatin regulation

What is the role of Pol II accumulation at the promoter-proximal region? Our analysis links promoter-proximal accumulation of Pol II with RNA surveillance and transcription termination. Binding of the RNA quality control factors Nab3, Mtr4 and Nab2 to mRNA transcripts is enhanced at promoter-proximal regions. Therefore, a model emerges that increased dwelling of Pol II at specific promoter-proximal sites provides the time for RNA surveillance and termination factors to be loaded to nascent transcripts efficiently. Our cumulative findings that in the absence of INO80 (i) Pol II accumulates at promoter proximal regions, (ii) Nab2 recruitment to chromatin and binding to RNA are defective and (iii) early termination is compromised, suggest that removal of Pol II molecules that are not engaged in productive transcription is mediated by INO80. Given that loss of INO80 results in reduced transcription rates, our results substantiate the hypothesis that chromatin promotes transcription by orchestrating the co-transcriptional RNA quality control pathway. It is therefore tempting to speculate that chromatin acts as a molecular switch that dictates whether Pol II will either progress into productive elongation or be removed to allow for the next round of transcription to take place.

Chromatin regulation of premature transcription termination by INO80

bioRxiv preprint doi: https://doi.org/10.1101/2020.03.02.973685; this version posted October 14, 2021. The copyright holder for this preprint (which was not certified by peer review) is the author/funder. All rights reserved. No reuse allowed without permission.

How does INO80 promote premature termination? The physical interactions of the INO80 complex with the transcription termination and RNA surveillance factors Nrd1 and Nab2, and the enrichment of INO80 at NNS-dependent termination regions suggest a direct involvement for INO80 in the co-transcriptional RNA quality control pathway. Nab2 associates with the RNA cleavage factor Hrp1[70] and both factors are involved in mRNA quality control and NNS-dependent termination[4,71,72]. The INO80-dependent recruitment of Nab2 to chromatin could therefore promote co-transcriptional cleavage of the nascent RNA, leading to destabilization of the transcription elongation complex and subsequent release of Pol II from chromatin. As INO80 interacts with and facilitates release of poly-ubiquitinated Rpb1 from chromatin[35], an intriguing possibility is that Rpb1 ubiquitination is involved in the process, providing specificity for selective eviction of Pol II molecules by INO80.

In agreement with a role for H2A.Z in RNA quality control and non-poly(A) transcription termination[64-66], our results suggest that INO80 promotes recruitment of Nab2 to chromatin by regulating its interaction with H2A.Z (Figure 7). This implies that remodelling of H2A.Z-containing nucleosomes by INO80[67-69] is important for premature termination. It is therefore likely that intermediate steps in the H2A.Z exchange reaction by INO80, for example disposing of DNA from the surface of H2A.Z-H2B dimers[69], might be involved in the process. How H2A.Z promotes recruitment of the RNA quality control machinery to chromatin is not clear. It would not be surprising if regulation of premature termination entails posttranslational modifications on H2A.Z, which would command its role in the RNA quality control pathway.

Promoter-proximal transcriptional pausing has recently been linked to premature termination in metazoans[6,19-21]. Uncontrolled transcription elongation and dysregulated Pol II pausing have been implicated in human disease[73,74]. Mutations in the RNA surveillance machinery have been associated with increased transcriptional stress and genomic instability[75], both

bioRxiv preprint doi: https://doi.org/10.1101/2020.03.02.973685; this version posted October 14, 2021. The copyright holder for this preprint (which was not certified by peer review) is the author/funder. All rights reserved. No reuse allowed without permission.

373 hallmarks of cancer[76]. Dysregulated expression of INO80 leads to uncontrolled gene
374 expression and is associated with disease[31,77,78]. We therefore anticipated that our reported
375 chromatin mechanism of co-transcriptional RNA quality control has general relevance for
376 regulation of eukaryotic gene expression and in disease.

bioRxiv preprint doi: https://doi.org/10.1101/2020.03.02.973685; this version posted October 14, 2021. The copyright holder for this preprint (which was not certified by peer review) is the author/funder. All rights reserved. No reuse allowed without permission.

Competing interests

The authors declare that they have no competing interests. BFP has a financial interest in Peconic, LLC, which utilizes the ChIP-exo technology implemented in this study and could potentially benefit from the outcomes of this research.

Funding

MPC is supported by Newcastle and Liverpool University. AM is supported by the Agence Nationale de la Recherche (ANR) (DNA-Life) and the European Research Council (EPIncRNA starting grant, DARK consolidator grant). This work has received support from the U.S. National Institutes of Health HG004160 to BFP, and from the ANR (AAPG2019 PICen to L.T., ANR-18-CE12-0026 and ANR-20-CE12-0014-02 to D.D.).

Acknowledgements

We thank D. Shapira (Newcastle University) for assisting with experiments and constructive discussions. We thank S. Baulande and P. Legoix-Né (NGS platform, Institute Curie). We also thank Maxime Wéry and Nicolas Vogt for outstanding help with the NET-seq and RNA-seq assays and critical reading of the manuscript, David A. Brow for the generous gift of the pGAC24 and pGAC24-SNR13TTS plasmids and the *nrd1-5* yeast strain, and Kuangyu Yen, Lisa Prendergast and members of the Papamichos-Chronakis and Morillon's labs for constructive discussions. This work has benefited from the facilities and expertise of the NGS platform of Institute Curie, supported by the Agence Nationale de la Recherche (ANR-10-EQPX-03, ANR10-INBS-09-08) and the Canceropôle Ile-de-France.

bioRxiv preprint doi: https://doi.org/10.1101/2020.03.02.973685; this version posted October 14, 2021. The copyright holder for this preprint (which was not certified by peer review) is the author/funder. All rights reserved. No reuse allowed without permission.

References

1. Porrua, O. & Libri, D. RNA quality control in the nucleus: the Angels' share of RNA. *Biochim Biophys Acta* **1829**, 604-11 (2013).
2. Pelechano, V., Chavez, S. & Perez-Ortin, J.E. A complete set of nascent transcription rates for yeast genes. *PLoS One* **5**, e15442 (2010).
3. Kim, T.S. et al. RNA polymerase mapping during stress responses reveals widespread nonproductive transcription in yeast. *Genome Biol* **11**, R75 (2010).
4. Tuck, A.C. & Tollervey, D. A transcriptome-wide atlas of RNP composition reveals diverse classes of mRNAs and lncRNAs. *Cell* **154**, 996-1009 (2013).
5. Bresson, S. & Tollervey, D. Surveillance-ready transcription: nuclear RNA decay as a default fate. *Open Biol* **8**(2018).
6. Steurer, B. et al. Live-cell analysis of endogenous GFP-RPB1 uncovers rapid turnover of initiating and promoter-paused RNA Polymerase II. *Proc Natl Acad Sci U S A* **115**, E4368-E4376 (2018).
7. Darzacq, X. et al. In vivo dynamics of RNA polymerase II transcription. *Nat Struct Mol Biol* **14**, 796-806 (2007).
8. Steinmetz, E.J., Conrad, N.K., Brow, D.A. & Corden, J.L. RNA-binding protein Nrd1 directs poly(A)-independent 3'-end formation of RNA polymerase II transcripts. *Nature* **413**, 327-31 (2001).
9. Kilchert, C., Wittmann, S. & Vasiljeva, L. The regulation and functions of the nuclear RNA exosome complex. *Nat Rev Mol Cell Biol* **17**, 227-39 (2016).
10. Jensen, T.H., Jacquier, A. & Libri, D. Dealing with pervasive transcription. *Mol Cell* **52**, 473-84 (2013).
11. Mayer, A. et al. CTD tyrosine phosphorylation impairs termination factor recruitment to RNA polymerase II. *Science* **336**, 1723-5 (2012).
12. Gonzalez-Aguilera, C. et al. Nab2 functions in the metabolism of RNA driven by polymerases II and III. *Mol Biol Cell* **22**, 2729-40 (2011).
13. Yu, M.C. et al. Arginine methyltransferase affects interactions and recruitment of mRNA processing and export factors. *Genes Dev* **18**, 2024-35 (2004).
14. Bresson, S., Tuck, A., Staneva, D. & Tollervey, D. Nuclear RNA Decay Pathways Aid Rapid Remodeling of Gene Expression in Yeast. *Mol Cell* **65**, 787-800 e5 (2017).
15. Webb, S., Hector, R.D., Kudla, G. & Granneman, S. PAR-CLIP data indicate that Nrd1-Nab3-dependent transcription termination regulates expression of hundreds of protein coding genes in yeast. *Genome Biol* **15**, R8 (2014).
16. Schulz, D. et al. Transcriptome surveillance by selective termination of noncoding RNA synthesis. *Cell* **155**, 1075-87 (2013).
17. Kapranov, P. et al. RNA maps reveal new RNA classes and a possible function for pervasive transcription. *Science* **316**, 1484-8 (2007).
18. Yu, D., Ma, X., Zuo, Z., Wang, H. & Meng, Y. Classification of Transcription Boundary-Associated RNAs (TBARs) in Animals and Plants. *Front Genet* **9**, 168 (2018).
19. Chiu, A.C. et al. Transcriptional Pause Sites Delineate Stable Nucleosome-Associated Premature Polyadenylation Suppressed by U1 snRNP. *Mol Cell* **69**, 648-663 e7 (2018).
20. Erickson, B., Sheridan, R.M., Cortazar, M. & Bentley, D.L. Dynamic turnover of paused Pol II complexes at human promoters. *Genes Dev* (2018).

bioRxiv preprint doi: https://doi.org/10.1101/2020.03.02.973685; this version posted October 14, 2021. The copyright holder for this preprint (which was not certified by peer review) is the author/funder. All rights reserved. No reuse allowed without permission.

21. Krebs, A.R. et al. Genome-wide Single-Molecule Footprinting Reveals High RNA Polymerase II Turnover at Paused Promoters. *Mol Cell* **67**, 411-422 e4 (2017).
22. Gressel, S. et al. CDK9-dependent RNA polymerase II pausing controls transcription initiation. *Elife* **6**(2017).
23. Shao, W. & Zeitlinger, J. Paused RNA polymerase II inhibits new transcriptional initiation. *Nat Genet* **49**, 1045-1051 (2017).
24. Chen, F.X., Smith, E.R. & Shilatifard, A. Born to run: control of transcription elongation by RNA polymerase II. *Nat Rev Mol Cell Biol* (2018).
25. Taft, R.J., Kaplan, C.D., Simons, C. & Mattick, J.S. Evolution, biogenesis and function of promoter-associated RNAs. *Cell Cycle* **8**, 2332-8 (2009).
26. Whitehouse, I., Rando, O.J., Delrow, J. & Tsukiyama, T. Chromatin remodelling at promoters suppresses antisense transcription. *Nature* **450**, 1031-5 (2007).
27. Boeger, H., Griesenbeck, J. & Kornberg, R.D. Nucleosome retention and the stochastic nature of promoter chromatin remodeling for transcription. *Cell* **133**, 716-26 (2008).
28. Smolle, M. et al. Chromatin remodelers Isw1 and Chd1 maintain chromatin structure during transcription by preventing histone exchange. *Nat Struct Mol Biol* **19**, 884-92 (2012).
29. Morillon, A. et al. Isw1 chromatin remodeling ATPase coordinates transcription elongation and termination by RNA polymerase II. *Cell* **115**, 425-35 (2003).
30. Babour, A. et al. The Chromatin Remodeler ISW1 Is a Quality Control Factor that Surveys Nuclear mRNP Biogenesis. *Cell* **167**, 1201-1214 e15 (2016).
31. Poli, J., Gasser, S.M. & Papamichos-Chronakis, M. The INO80 remodeller in transcription, replication and repair. *Philos Trans R Soc Lond B Biol Sci* **372**(2017).
32. Xue, Y. et al. Mot1, Ino80C, and NC2 Function Coordinately to Regulate Pervasive Transcription in Yeast and Mammals. *Mol Cell* **67**, 594-607 e4 (2017).
33. Yen, K., Vinayachandran, V. & Pugh, B.F. SWR-C and INO80 chromatin remodelers recognize nucleosome-free regions near +1 nucleosomes. *Cell* **154**, 1246-56 (2013).
34. Poli, J. et al. Mec1, INO80, and the PAF1 complex cooperate to limit transcription replication conflicts through RNAPII removal during replication stress. *Genes Dev* **30**, 337-54 (2016).
35. Lafon, A. et al. INO80 Chromatin Remodeler Facilitates Release of RNA Polymerase II from Chromatin for Ubiquitin-Mediated Proteasomal Degradation. *Mol Cell* **60**, 784-96 (2015).
36. Tsvetanova, N.G., Klass, D.M., Salzman, J. & Brown, P.O. Proteome-wide search reveals unexpected RNA-binding proteins in Saccharomyces cerevisiae. *PLoS One* **5**(2010).
37. Edupuganti, R.R. et al. N(6)-methyladenosine (m(6)A) recruits and repels proteins to regulate mRNA homeostasis. *Nat Struct Mol Biol* **24**, 870-878 (2017).
38. Churchman, L.S. & Weissman, J.S. Nascent transcript sequencing visualizes transcription at nucleotide resolution. *Nature* **469**, 368-73 (2011).
39. Wissink, E.M., Vihervaara, A., Tippens, N.D. & Lis, J.T. Nascent RNA analyses: tracking transcription and its regulation. *Nat Rev Genet* (2019).
40. Harlen, K.M. & Churchman, L.S. Subgenic Pol II interactomes identify region-specific transcription elongation regulators. *Mol Syst Biol* **13**, 900 (2017).

bioRxiv preprint doi: https://doi.org/10.1101/2020.03.02.973685; this version posted October 14, 2021. The copyright holder for this preprint (which was not certified by peer review) is the author/funder. All rights reserved. No reuse allowed without permission.

41. Yen, K., Vinayachandran, V., Batta, K., Koerber, R.T. & Pugh, B.F. Genome-wide nucleosome specificity and directionality of chromatin remodelers. *Cell* **149**, 1461-73 (2012).
42. Rhee, H.S. & Pugh, B.F. ChIP-exo method for identifying genomic location of DNA-binding proteins with near-single-nucleotide accuracy. *Curr Protoc Mol Biol* **Chapter 21**, Unit 21 24 (2012).
43. Shaw, R.J. & Reines, D. Saccharomyces cerevisiae transcription elongation mutants are defective in PUR5 induction in response to nucleotide depletion. *Mol Cell Biol* **20**, 7427-37 (2000).
44. Ehrensberger, A.H., Kelly, G.P. & Svejstrup, J.Q. Mechanistic interpretation of promoter-proximal peaks and RNAPII density maps. *Cell* **154**, 713-5 (2013).
45. Baptista, T. et al. SAGA Is a General Cofactor for RNA Polymerase II Transcription. *Mol Cell* **68**, 130-143 e5 (2017).
46. Timmers, H.T.M. & Tora, L. Transcript Buffering: A Balancing Act between mRNA Synthesis and mRNA Degradation. *Mol Cell* **72**, 10-17 (2018).
47. Sun, M. et al. Comparative dynamic transcriptome analysis (cDTA) reveals mutual feedback between mRNA synthesis and degradation. *Genome Res* **22**, 1350-9 (2012).
48. Malagon, F. et al. Mutations in the Saccharomyces cerevisiae RPB1 gene conferring hypersensitivity to 6-azauracil. *Genetics* **172**, 2201-9 (2006).
49. Pelechano, V. & Perez-Ortin, J.E. The transcriptional inhibitor thiolutin blocks mRNA degradation in yeast. *Yeast* **25**, 85-92 (2008).
50. Alpert, T., Straube, K., Carrillo Oesterreich, F., Herzel, L. & Neugebauer, K.M. Widespread Transcriptional Readthrough Caused by Nab2 Depletion Leads to Chimeric Transcripts with Retained Introns. *Cell Rep* **33**, 108324 (2020).
51. Aguilar, L.C. et al. Altered rRNA processing disrupts nuclear RNA homeostasis via competition for the poly(A)-binding protein Nab2. *Nucleic Acids Res* **48**, 11675-11694 (2020).
52. Fasken, M.B., Laribee, R.N. & Corbett, A.H. Nab3 facilitates the function of the TRAMP complex in RNA processing via recruitment of Rrp6 independent of Nrd1. *PLoS Genet* **11**, e1005044 (2015).
53. Fox, M.J. & Mosley, A.L. Rrp6: Integrated roles in nuclear RNA metabolism and transcription termination. *Wiley Interdiscip Rev RNA* **7**, 91-104 (2016).
54. Vasiljeva, L. & Buratowski, S. Nrd1 interacts with the nuclear exosome for 3' processing of RNA polymerase II transcripts. *Mol Cell* **21**, 239-48 (2006).
55. Tudek, A. et al. Molecular basis for coordinating transcription termination with noncoding RNA degradation. *Mol Cell* **55**, 467-81 (2014).
56. Holmes, R.K. et al. Loss of the Yeast SR Protein Npl3 Alters Gene Expression Due to Transcription Readthrough. *PLoS Genet* **11**, e1005735 (2015).
57. Schwer, B., Mao, X. & Shuman, S. Accelerated mRNA decay in conditional mutants of yeast mRNA capping enzyme. *Nucleic Acids Res* **26**, 2050-7 (1998).
58. Breslow, D.K. et al. A comprehensive strategy enabling high-resolution functional analysis of the yeast genome. *Nat Methods* **5**, 711-8 (2008).
59. Arigo, J.T., Carroll, K.L., Ames, J.M. & Corden, J.L. Regulation of yeast NRD1 expression by premature transcription termination. *Mol Cell* **21**, 641-51 (2006).
60. Kim, M. et al. Distinct pathways for snoRNA and mRNA termination. *Mol Cell* **24**, 723-734 (2006).

bioRxiv preprint doi: https://doi.org/10.1101/2020.03.02.973685; this version posted October 14, 2021. The copyright holder for this preprint (which was not certified by peer review) is the author/funder. All rights reserved. No reuse allowed without permission.

61. Fox, M.J., Gao, H., Smith-Kinnaman, W.R., Liu, Y. & Mosley, A.L. The exosome component Rrp6 is required for RNA polymerase II termination at specific targets of the Nrd1-Nab3 pathway. *PLoS Genet* **11**, e1004999 (2015).
62. van Dijk, E.L. et al. XUTs are a class of Xrn1-sensitive antisense regulatory non-coding RNA in yeast. *Nature* **475**, 114-7 (2011).
63. Albert, I. et al. Translational and rotational settings of H2A.Z nucleosomes across the Saccharomyces cerevisiae genome. *Nature* **446**, 572-6 (2007).
64. Zofall, M. et al. Histone H2A.Z cooperates with RNAi and heterochromatin factors to suppress antisense RNAs. *Nature* **461**, 419-22 (2009).
65. Wagner, E.J. et al. A genome-wide RNA interference screen reveals that variant histones are necessary for replication-dependent histone pre-mRNA processing. *Mol Cell* **28**, 692-9 (2007).
66. Muniz, L. et al. Control of Gene Expression in Senescence through Transcriptional Read-Through of Convergent Protein-Coding Genes. *Cell Rep* **21**, 2433-2446 (2017).
67. Papamichos-Chronakis, M., Watanabe, S., Rando, O.J. & Peterson, C.L. Global regulation of H2A.Z localization by the INO80 chromatin-remodeling enzyme is essential for genome integrity. *Cell* **144**, 200-13 (2011).
68. Eustermann, S. et al. Structural basis for ATP-dependent chromatin remodelling by the INO80 complex. *Nature* **556**, 386-390 (2018).
69. Brahma, S. et al. INO80 exchanges H2A.Z for H2A by translocating on DNA proximal to histone dimers. *Nat Commun* **8**, 15616 (2017).
70. Dheur, S., Nykamp, K.R., Viphakone, N., Swanson, M.S. & Minvielle-Sebastia, L. Yeast mRNA Poly(A) tail length control can be reconstituted in vitro in the absence of Pab1p-dependent Poly(A) nuclease activity. *J Biol Chem* **280**, 24532-8 (2005).
71. Kuehner, J.N. & Brow, D.A. Regulation of a eukaryotic gene by GTP-dependent start site selection and transcription attenuation. *Mol Cell* **31**, 201-11 (2008).
72. Roth, K.M., Wolf, M.K., Rossi, M. & Butler, J.S. The nuclear exosome contributes to autogenous control of NAB2 mRNA levels. *Mol Cell Biol* **25**, 1577-85 (2005).
73. Rahl, P.B. et al. c-Myc regulates transcriptional pause release. *Cell* **141**, 432-45 (2010).
74. Zhang, X. et al. Attenuation of RNA polymerase II pausing mitigates BRCA1-associated R-loop accumulation and tumorigenesis. *Nat Commun* **8**, 15908 (2017).
75. Aguilera, A. & Gomez-Gonzalez, B. Genome instability: a mechanistic view of its causes and consequences. *Nat Rev Genet* **9**, 204-17 (2008).
76. Kotsantis, P., Petermann, E. & Boulton, S.J. Mechanisms of Oncogene-Induced Replication Stress: Jigsaw Falling into Place. *Cancer Discov* **8**, 537-555 (2018).
77. Zhou, B. et al. INO80 governs superenhancer-mediated oncogenic transcription and tumor growth in melanoma. *Genes Dev* **30**, 1440-53 (2016).
78. Zhang, S. et al. INO80 is required for oncogenic transcription and tumor growth in non-small cell lung cancer. *Oncogene* **36**, 1430-1439 (2017).
79. Hemming, S.A. et al. RNA polymerase II subunit Rpb9 regulates transcription elongation in vivo. *J Biol Chem* **275**, 35506-11 (2000).
80. Riles, L., Shaw, R.J., Johnston, M. & Reines, D. Large-scale screening of yeast mutants for sensitivity to the IMP dehydrogenase inhibitor 6-azauracil. *Yeast* **21**, 241-8 (2004).

bioRxiv preprint doi: https://doi.org/10.1101/2020.03.02.973685; this version posted October 14, 2021. The copyright holder for this preprint (which was not certified by peer review) is the author/funder. All rights reserved. No reuse allowed without permission.

81. Creamer, T.J. et al. Transcriptome-wide binding sites for components of the Saccharomyces cerevisiae non-poly(A) termination pathway: Nrd1, Nab3, and Sen1. *PLoS Genet* **7**, e1002329 (2011).
82. Jonsson, Z.O., Jha, S., Wohlschlegel, J.A. & Dutta, A. Rvb1p/Rvb2p recruit Arp5p and assemble a functional Ino80 chromatin remodeling complex. *Mol Cell* **16**, 465-77 (2004).
83. Wery, M. et al. Nonsense-Mediated Decay Restricts LncRNA Levels in Yeast Unless Blocked by Double-Stranded RNA Structure. *Mol Cell* **61**, 379-392 (2016).
84. Wery, M. et al. Native elongating transcript sequencing reveals global anti-correlation between sense and antisense nascent transcription in fission yeast. *RNA* **24**, 196-208 (2018).
85. Baptista, T. & Devys, D. Saccharomyces cerevisiae Metabolic Labeling with 4-thiouracil and the Quantification of Newly Synthesized mRNA As a Proxy for RNA Polymerase II Activity. *J Vis Exp* (2018).
86. Papamichos-Chronakis, M. & Peterson, C.L. The Ino80 chromatin-remodeling enzyme regulates replisome function and stability. *Nat Struct Mol Biol* **15**, 338-45 (2008).
87. Rhee, H.S., Bataille, A.R., Zhang, L. & Pugh, B.F. Subnucleosomal structures and nucleosome asymmetry across a genome. *Cell* **159**, 1377-88 (2014).

bioRxiv preprint doi: https://doi.org/10.1101/2020.03.02.973685; this version posted October 14, 2021. The copyright holder for this preprint (which was not certified by peer review) is the author/funder. All rights reserved. No reuse allowed without permission.

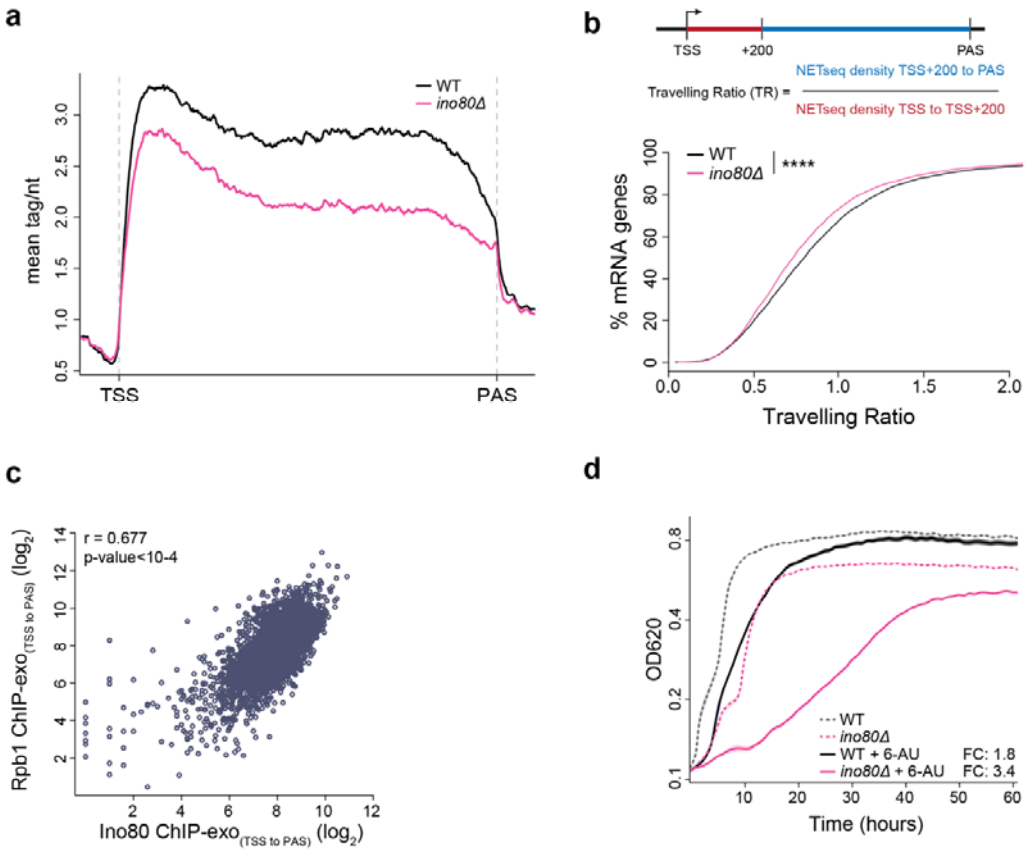


Fig. 1. Accumulation of nascent mRNA transcripts on chromatin proximally to promoters and defective transcriptional elongation in the absence of INO80.

a, Metagene analysis for NET-seq density profiles averaged across scaled mRNA genes (n= 5432) in WT and *ino80Δ*. Tags were aligned to both Transcription Start Site (TSS) and Polyadenylation Site (PAS) for each gene. n=2. **b,** Top: Schematic representation and formula for calculating the Traveling Ratio (TR) from NET-seq mRNA densities. Bottom: Cumulative distribution plot of Traveling Ratio for mRNA genes from a (n=5432). Genes with TR>2 (WT: n=354, *ino80Δ*: n=314) are not shown. ****p < 0.0XXX with K-S test. **c,** Scatterplot analysis comparing Ino80[33] and Rpb1 ChIP-exo densities between the transcription start site and polyadenylation site (TSS to PAS) in mRNA yeast genes (n=5798). Pearson's correlation coefficient (r) and p-value are indicated. **d,** Cell proliferation

bioRxiv preprint doi: https://doi.org/10.1101/2020.03.02.973685; this version posted October 14, 2021. The copyright holder for this preprint (which was not certified by peer review) is the author/funder. All rights reserved. No reuse allowed without permission.

610 analysis for WT and *ino80Δ* strains grown exponentially in SC-ura and in SC-ura containing
611 50 µg/ml 6-azauracil (6-AU) liquid media for the indicated time. Cell density was measured
612 at OD^{620} and plotted on a $\log_2$ scale. Doubling time was calculated from OD^{620}: 0.2 to OD^{620}:
613 0.4 for all strains in both conditions. Fold Change ratio (FC) of doubling time in 6-AU over
614 SC-ura for each strain is shown. n=4.

bioRxiv preprint doi: https://doi.org/10.1101/2020.03.02.973685; this version posted October 14, 2021. The copyright holder for this preprint (which was not certified by peer review) is the author/funder. All rights reserved. No reuse allowed without permission.

Figure 3

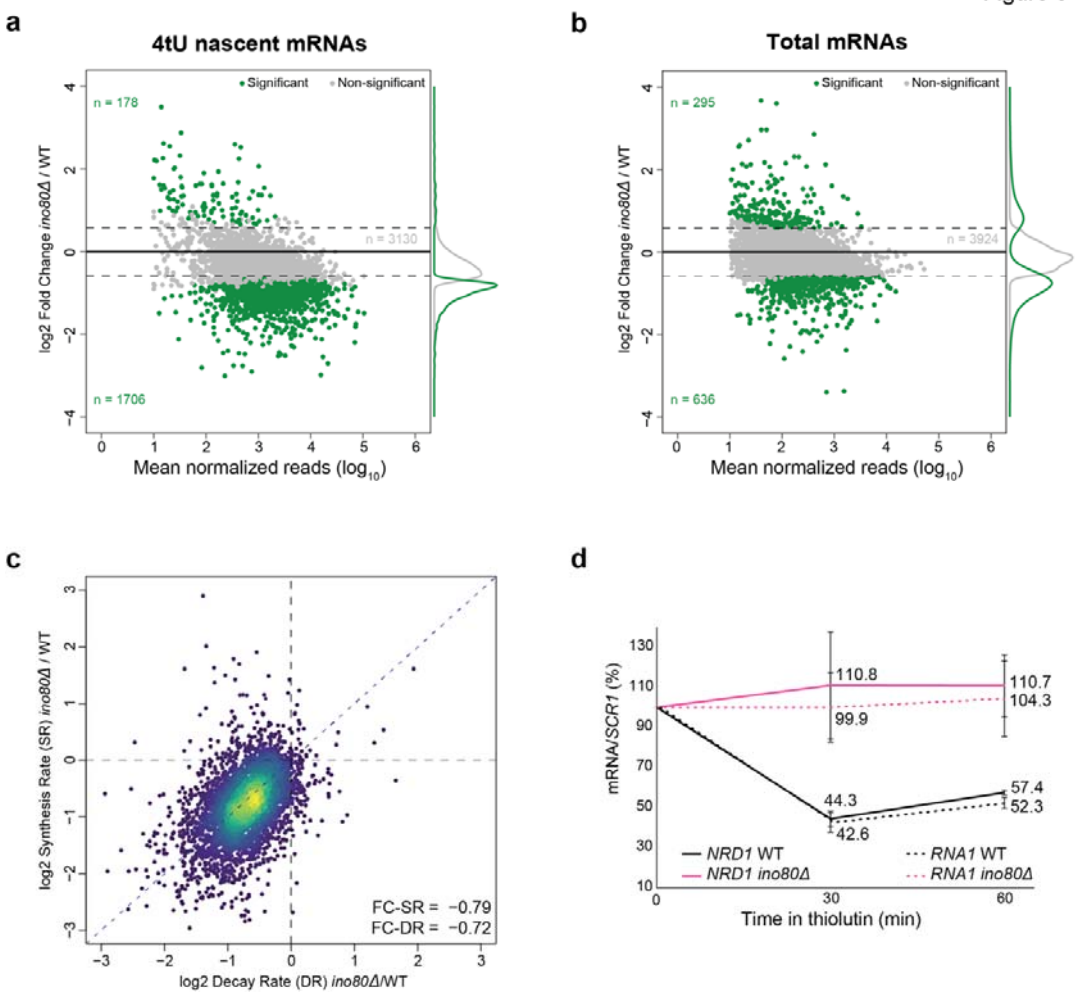


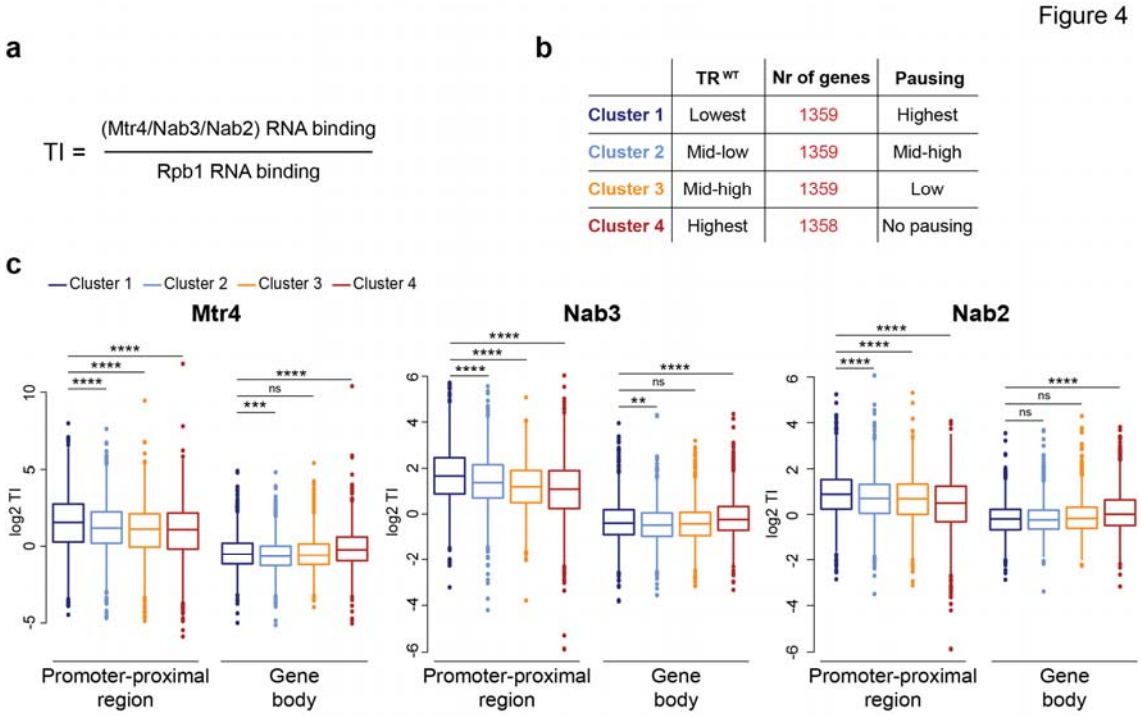
Fig. 3. mRNA synthesis and decay rates are reduced in the absence of INO80.

a, b, Scatterplot analysis for fold changes between WT and *ino80Δ* in newly synthesized mRNA (a) and steady-state mRNA (b) levels (n=5012 genes) plotted on a $\log_2$ scale. Thresholds of 1.5-fold change and 0.05 p values were considered for significant change (green dots). n=3. **c,** cDTA profiles for *ino80Δ*. For all analysed genes, changes in synthesis rates (SR) were plotted against the changes in mRNA decay rates (DR). Fold-change in SR and DR were calculated between *ino80Δ* and WT and plotted on a $\log_2$ scale. 90% of genes are contained within the outer contour. Yellow and red dots correspond to 60% of genes. **d,** RT-qPCR analysis for *NRD1* and *RNA1* RNAs was conducted in WT and *ino80Δ* before (T_0) and after addition of thiolutin in YPD. RNA abundance at each time-point was normalized

bioRxiv preprint doi: https://doi.org/10.1101/2020.03.02.973685; this version posted October 14, 2021. The copyright holder for this preprint (which was not certified by peer review) is the author/funder. All rights reserved. No reuse allowed without permission.

626 over the respective abundance of the *SCR1* RNA. RNA before thiolutin treatment was set at
627 100% in both strains. Remaining RNA was calculated as the amount of normalized RNA in
628 the indicated time-points relative to the normalized RNA at T_0. Values represent the average
629 from at least three independent experiments. Bars, standard errors.

Figure 4



630

631

632 **Fig. 4. Loading of the RNA surveillance and termination factors Mtr4, Nab3 and Nab2**
633 **on promoter-proximal mRNA transcripts.**

634 **a,** Formula for calculating Transcript Instability (TI) as the ratio of the averaged CRAC
635 densities of Nab3[56], Mtr4 or Nab2[4] to CRAC densities of Rpb1[56] for mRNA genes. **b,**
636 Schematic table for clustering mRNA genes according to the relative TR in WT (TR^{WT}). The
637 number of genes and the level of promoter-proximal pausing are indicated for each cluster. **c,**
638 Boxplot analysis comparing TIs calculated for the promoter-proximal and gene body regions
639 of mRNA genes in the four clusters defined by their relative TR^{WT}. p-values were calculated
640 by Wilcoxon rank-sum test. ****, $p<0.0001$. ***, $p<0.001$. **, $p<0.01$. ns, non-significant.

bioRxiv preprint doi: https://doi.org/10.1101/2020.03.02.973685; this version posted October 14, 2021. The copyright holder for this preprint (which was not certified by peer review) is the author/funder. All rights reserved. No reuse allowed without permission.

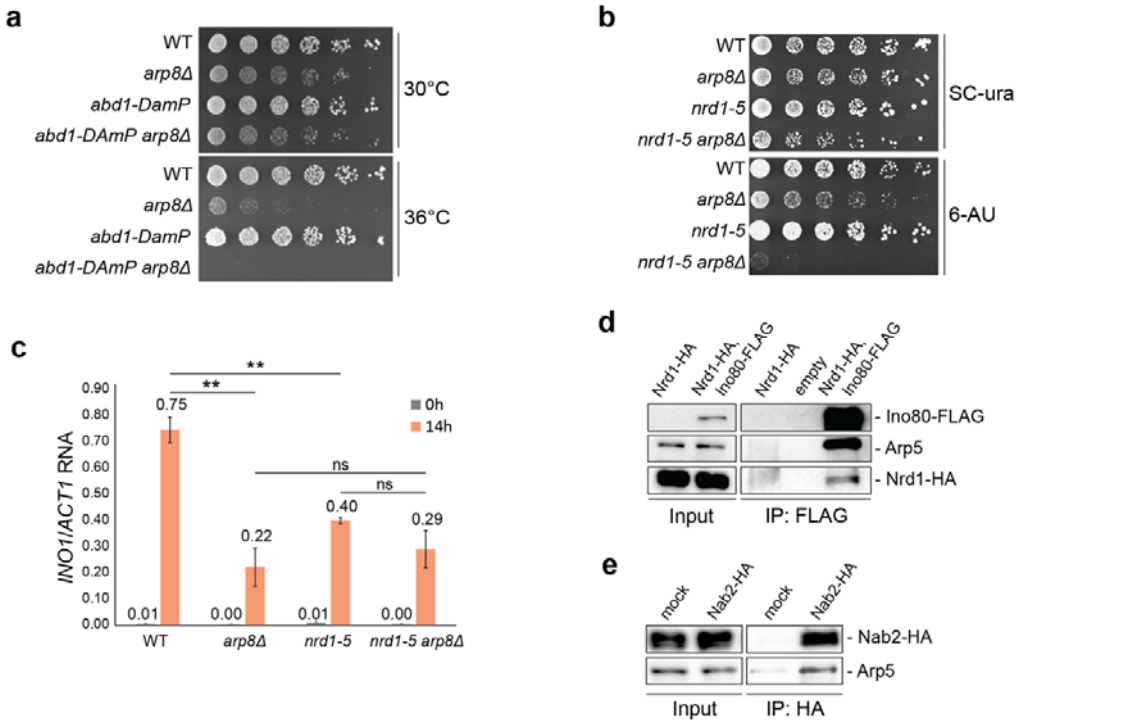


Fig. 5. Genetic and physical interactions of INO80 with the RNA quality control pathway.

a, 5-fold serial dilution of exponentially grown cells from the indicated strains were plated onto YPD and incubated at 30°C (permissive temperature) or 37°C (non-permissive temperature) for 4-5 days. **b,** 5-fold serial dilution of exponentially grown cells from the indicated strains were plated onto both SC-ura and SC-ura + 50µg/ml 6-Azauracil (6-AU) and incubated at 30°C for 4-5 days. **c,** RT-qPCR analysis for *INO1* RNA was conducted in the indicated strains grown exponentially in SC media (0h) or SC without inositol for 14h. *INO1* RNA was normalized over *ACT1* RNA. Bars, standard errors (n=3). Asterisks indicate statistical significance of the indicated change as calculated by Tukey's multiple comparisons test. ns: non-significant. **d,** Nucleic acid-free lysates from cells co-expressing Nrd1-HA with Ino80 either untagged or tagged with FLAG epitope were subjected to FLAG-IP. Inputs and IP samples were immunoblotted for FLAG, Arp5, HA. Immunoblot against Pgk1 served as a control. **E,** Nucleic acid-free lysates from cells expressing Nab2-HA were subjected to either

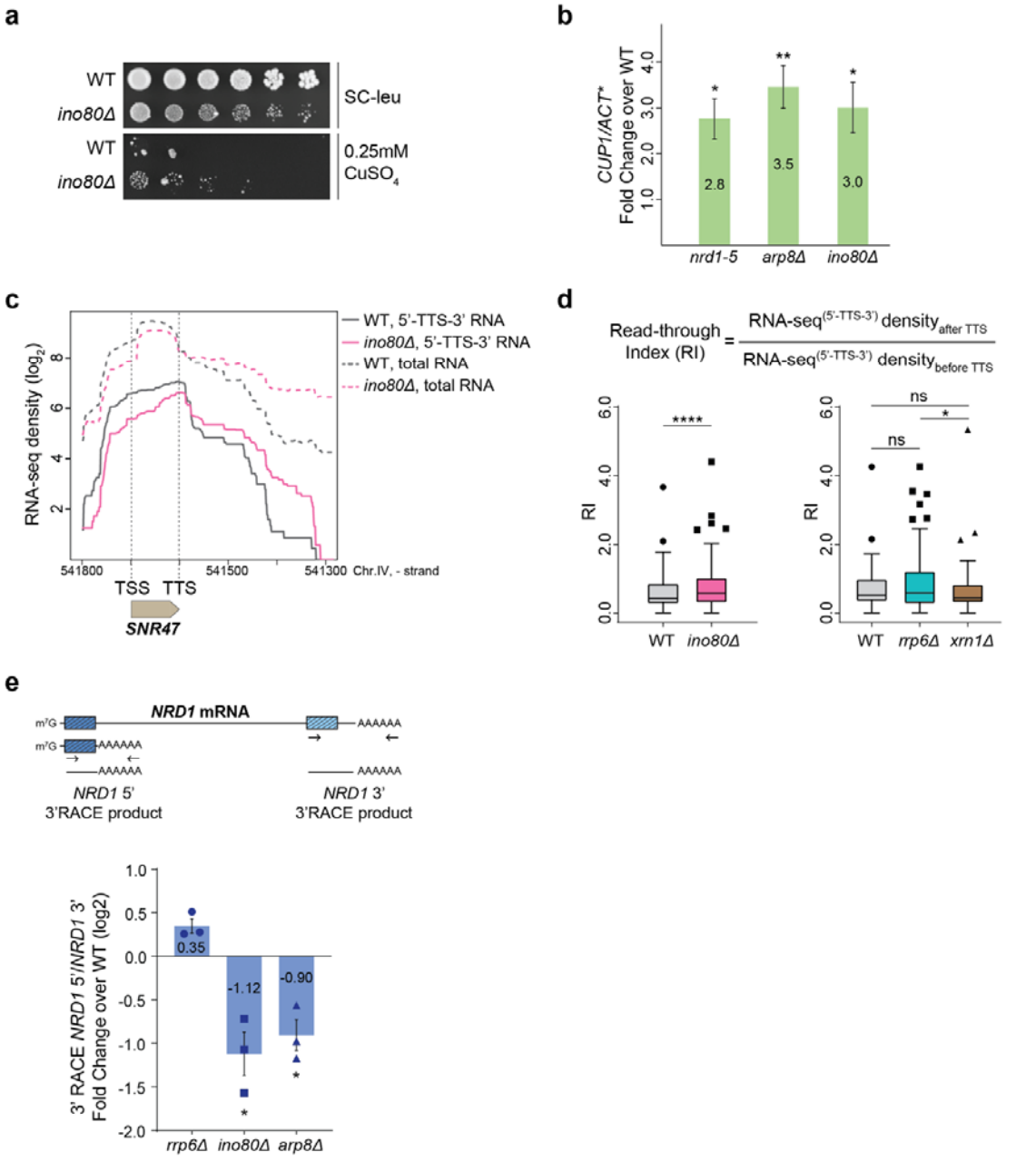
bioRxiv preprint doi: https://doi.org/10.1101/2020.03.02.973685; this version posted October 14, 2021. The copyright holder for this preprint (which was not certified by peer review) is the author/funder. All rights reserved. No reuse allowed without permission.

656 HA-IP (Nab2-HA) or IgG-IP (mock). Inputs and IP samples were immunoblotted for Arp5

657 and HA.

bioRxiv preprint doi: https://doi.org/10.1101/2020.03.02.973685; this version posted October 14, 2021. The copyright holder for this preprint (which was not certified by peer review) is the author/funder. All rights reserved. No reuse allowed without permission.

Figure 6



658

659 **Fig. 6. NNS-dependent transcriptional termination is defective in *ino80Δ*.**

660 **a,** 5-fold serial dilution of cells from the indicated strains were plated onto both SC-leu and

661 SC-leu + 0.25mM $CuSO_4$ and incubated at 30°C for 3 (SC-leu) and 7 days ($CuSO_4$). **b,** RT-

662 qPCR analysis was conducted in WT, *nrd1-5*, *arp8Δ* and *ino80Δ* cells transformed with

663 either *ACT-CUP* or *ACT-SNR^{TTS}-CUP* plasmids. The *CUP1*/*ACT** ratio from the *ACT-*

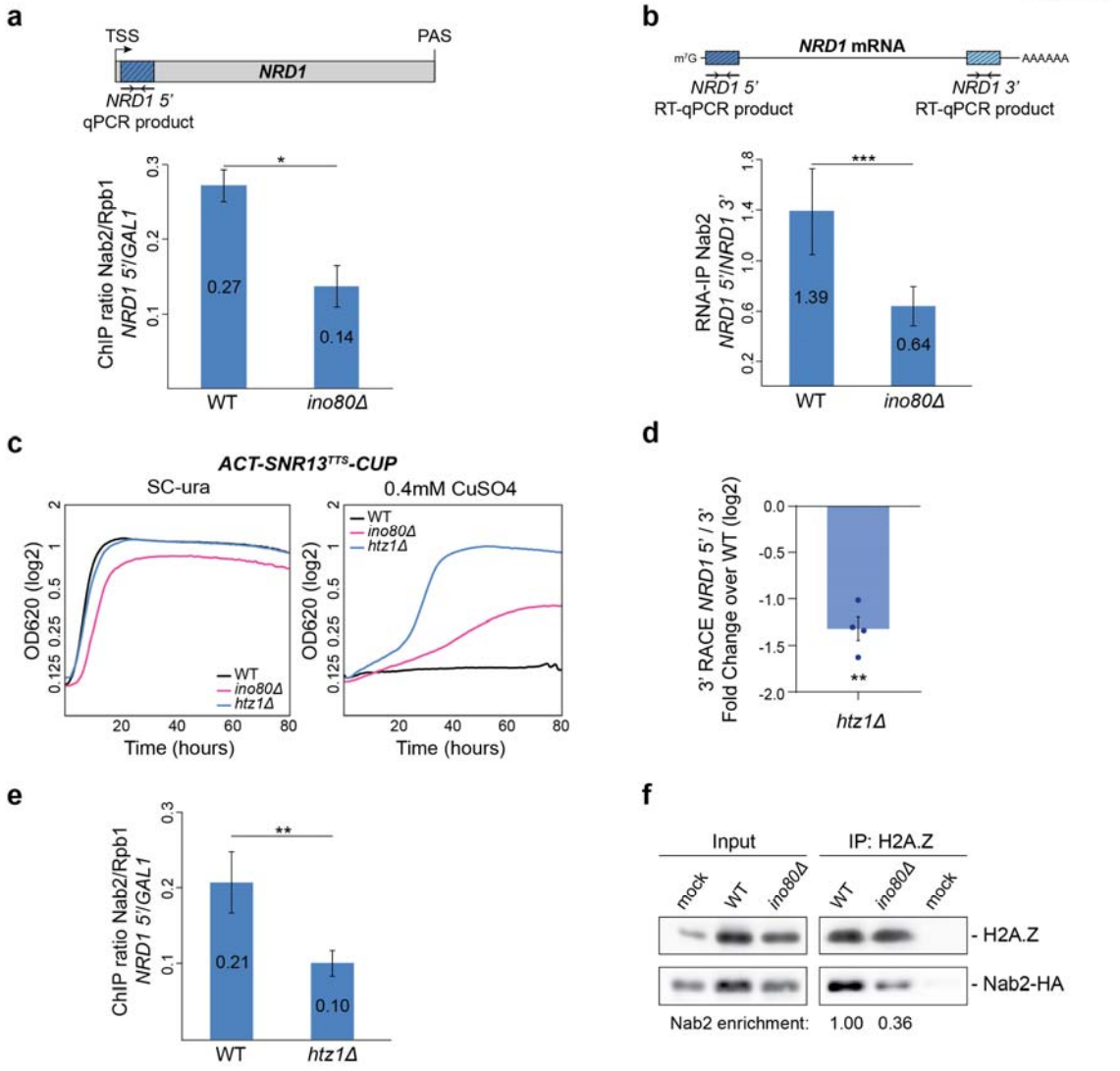
664 *SNR^{TTS}-CUP* plasmid was normalized over the same ratio from the control *ACT-CUP*

bioRxiv preprint doi: https://doi.org/10.1101/2020.03.02.973685; this version posted October 14, 2021. The copyright holder for this preprint (which was not certified by peer review) is the author/funder. All rights reserved. No reuse allowed without permission.

plasmid (Extended Fig. 4c) to correct for differential transcription across all strains. Read-through at the *SNR13*^{TTS} for each indicated strain is shown as Fold Change Ratio over WT. Bars, standard errors from three independent experiments. p-values were calculated by t-test after testing for normal distribution by Shapiro-Wilk test. *, p<0.05. **, p<0.01. **c,** Snapshot of RNA-seq densities in WT and *ino80Δ* across the *SNR47* snoRNA gene. Solid lines, density of reads encompassing the transcription termination site (5'-TTS-3') of the *SNR47* gene. Broken lines, total RNA-seq density. Reads encompassing the TTS were selected from the total RNA-seq reads as containing 5' upstream the *SNR47* TTS and 3' at or after the *SNR47* TTS. Genomic coordinates of Chromosome IV around the *SNR47* gene (coordinates: 541700 to 541602) are shown. The closest downstream gene is *YDR042C* (TSS: Chromosome IV, 541203). n=4. **d,** Upper panel, formula for calculating the Read-through Index (RI) from RNA-seq densities across snoRNA genes that encompass transcription termination sites (5'-TTS-3'). RNA-seq reads with 5' upstream the TTS and 3' at or after the TTS were selected from the total RNA-seq read pool and the ratio of the RNA-seq read density after TTS to the RNA-seq read density before TTS in the selected reads was calculated. Lower panel, boxplot analysis comparing RI from the indicated strains across snoRNA genes. p-values were calculated by Wilcoxon matched-pairs rank test after testing for normal distribution. ****, p<0.0001. *, p<0.05. ns, non-significant. **e,** Top: Scheme illustrating nested 3'RACE for termination events at the promoter-proximal (5') and PAS (3') regions of the *NRD1* gene (*NRD1 5'*, dark blue). Bottom: 3'RACE analysis for *NRD1* termination events was conducted in WT and the indicated mutant strains. The relative enrichment of polyadenylated promoter-proximal to PAS-terminated transcripts (5'/3') was calculated for all strains and the fold change in each mutant compared to WT was plotted on a $\log_2$ scale. n=3. p-values were calculated by t-test after testing for normal distribution by Shapiro-Wilk test. *, p<0.05.

bioRxiv preprint doi: https://doi.org/10.1101/2020.03.02.973685; this version posted October 14, 2021. The copyright holder for this preprint (which was not certified by peer review) is the author/funder. All rights reserved. No reuse allowed without permission.

Figure 7



689

690

691 **Fig. 7. INO80 promotes the co-transcriptional recruitment of Nab2 to chromatin and its**

692 **association with H2A.Z.**

693 **a,** Chromatin immunoprecipitation for Nab2-HA and Rpb1 in WT and *ino80Δ* cells. Fold

694 enrichment of each protein at the promoter-proximal region of *NRD1* gene (*NRD1 5'*) (upper

695 panel, shaded in dark blue) was calculated relative to the *GAL1* promoter after correction for

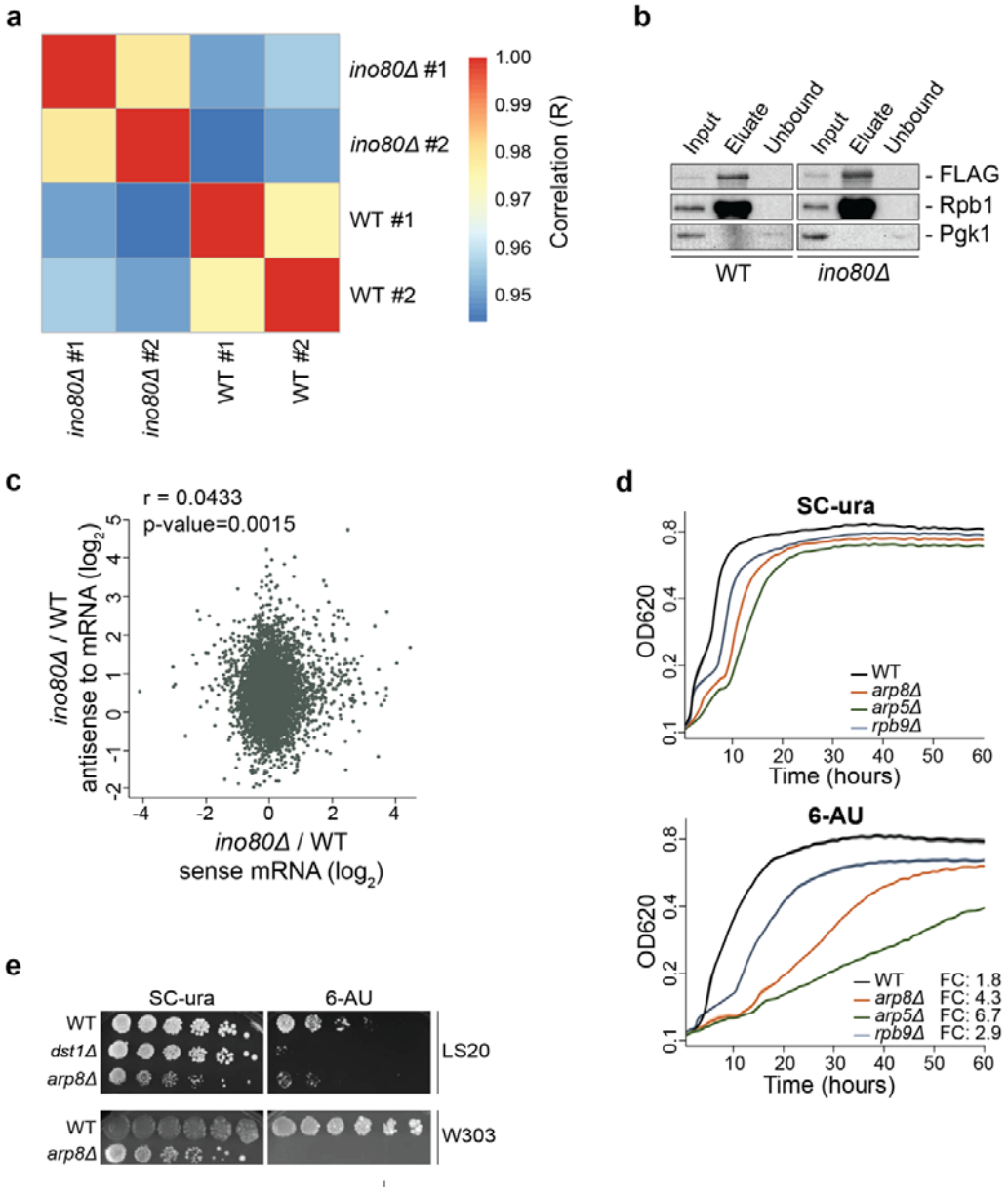
696 input DNA levels. ChIP ratio at the promoter-proximal region of *NRD1* gene (*NRD1 5'*) was

697 calculated as Fold enrichment of Nab2-HA over Fold enrichment of Rpb1. Bars, standard

bioRxiv preprint doi: https://doi.org/10.1101/2020.03.02.973685; this version posted October 14, 2021. The copyright holder for this preprint (which was not certified by peer review) is the author/funder. All rights reserved. No reuse allowed without permission.

errors from four independent experiments. p-values were calculated by t-test after testing for normal distribution by Shapiro-Wilk test. *, $p<0.05$. **b,** RNA immunoprecipitation for Nab2-HA in WT and *ino80Δ* cells. Ratio of binding of Nab2 to the promoter-proximal *NRD1* RNA (upper panel, *NRD1 5'*, dark blue) over binding to the 3' region of *NRD1* RNA (upper panel, *NRD1 3'*, light blue) after correction for input (total) RNA levels in the indicated strains. Bars, standard errors from four independent experiments. p-values were calculated by t-test after testing for normal distribution by Shapiro-Wilk test. ***, $p<0.001$. **c,** Cell proliferation analysis for the indicated strains transformed with the *ACT-SNR*^{TTS}*-CUP* plasmid grown exponentially in SC-ura (left panel) and in SC-ura liquid media containing 0.4mM $CuSO_4$ (6-AU) (right panel) for the indicated time. Cell density was measured at OD^{620} and is shown on a $\log_2$ scale. **d,** Nested 3'RACE analysis for termination events at the *NRD1* gene was conducted in WT and *htz1Δ*. Analysis was conducted as in Fig. 6e. n=4. p-values were calculated by t-test after testing for normal distribution by Shapiro-Wilk test. **, $p<0.01$. **e,** Chromatin immunoprecipitation for Nab2-HA and Rpb1 in WT and *htz1Δ* cells. Analysis was conducted as in (a). Bars, standard errors from three independent experiments. p-values were calculated by t-test after testing for normal distribution by Shapiro-Wilk test. **, $p<0.01$. **f,** Representative H2A.Z immunoprecipitation experiment. Nucleic acid-free lysates from WT and *ino80Δ* cells expressing Nab2-HA were subjected to H2A.Z-IP. Inputs and IP samples were immunoblotted for H2A.Z and HA. Nab2-HA enrichment in H2A.Z pulldowns is calculated as HA/H2A.Z IP ratio, corrected for the relative Nab2-HA abundance in the input samples. Nab2-HA enrichment in WT is set arbitrarily to 1.0. All analysis was conducted from the same SDS-page gel.

bioRxiv preprint doi: https://doi.org/10.1101/2020.03.02.973685; this version posted October 14, 2021. The copyright holder for this preprint (which was not certified by peer review) is the author/funder. All rights reserved. No reuse allowed without permission.



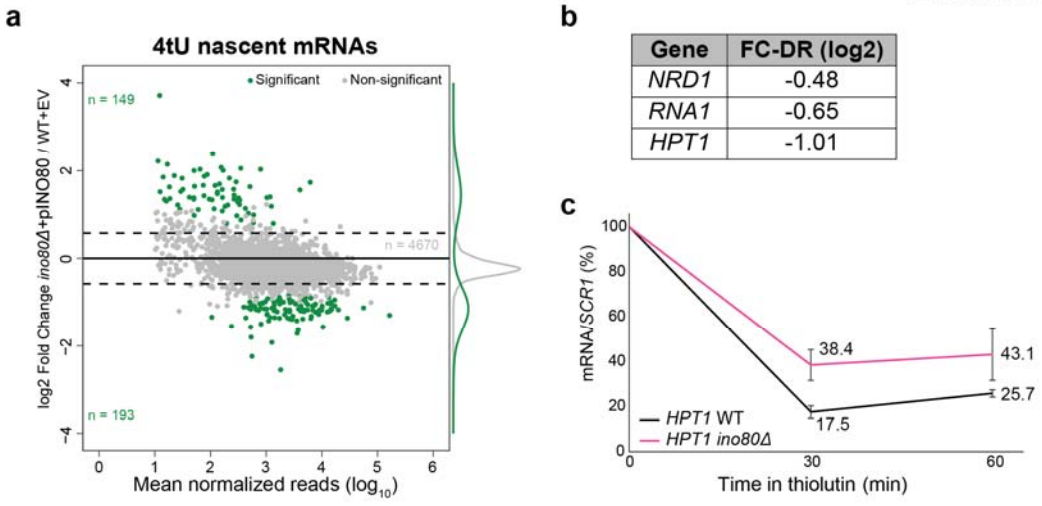
Extended Data Fig. 1. NET-seq and 6-AU cell growth analysis in the absence of INO80.

a, Heatmap of Pearson's correlation coefficients (R) for all pairwise combinations of NET-seq reads in independent biological replicates. **b,** Rpb1-FLAG is efficiently immunoprecipitated from yeast cells during NET-seq analysis. Lysates from WT and *ino80Δ* cells expressing *RPB1-FLAG* were subjected to FLAG immunoprecipitation using FLAG beads. Rpb1-FLAG was subsequently eluted from the beads with FLAG peptide. Input,

bioRxiv preprint doi: https://doi.org/10.1101/2020.03.02.973685; this version posted October 14, 2021. The copyright holder for this preprint (which was not certified by peer review) is the author/funder. All rights reserved. No reuse allowed without permission.

727 eluate and unbound samples were immunoblotted against FLAG epitope and total Rpb1.
728 Immunoblotting against Pgk1 serves as loading control. All samples were resolved in the
729 same SDS-page gel. **c,** Scatterplot analysis comparing the changes in NET-seq densities
730 between WT and *ino80Δ* for sense transcripts and their relative antisense transcripts over
731 mRNA gene regions, plotted on a $\log_2$ scale. Pearson's correlation coefficient (r) is indicated.
732 **d,** Cell proliferation analysis for the indicated strains grown exponentially in SC-ura (top
733 panel) and in SC-ura containing 50µg/ml 6-azauracil (6-AU) (bottom panel) liquid media for
734 the indicated time. Cell density was measured at OD^{620} and shown on a $\log_2$ scale. Shading
735 surrounding each line denotes standard error from four independent experiments. The mutant
736 strain deleted for the RNA Polymerase II subunit Rpb9 (*rpb9Δ*) has reported transcriptional
737 elongation defects in 6-AU[79] and was used as control. Doubling time from OD^{620} 0.2 to
738 OD^{620} 0.4 was calculated for all strains in both conditions. Fold Change ratio (FC) of
739 doubling time in 6-AU over SC-ura is shown (bottom panel). **e,** 5-fold serial dilution of cells
740 from the indicated strains were plated onto both SC-ura and SC-ura + 50µg/ml 6-Azauracil
741 (6-AU) and incubated at 30°C for 4-5 days. Genetic backgrounds (LS20, W303) are
742 indicated. The mutant strain deleted for the Dst1/TFIIS transcription elongation factor (*dst1Δ*)
743 was used as control[80].

bioRxiv preprint doi: https://doi.org/10.1101/2020.03.02.973685; this version posted October 14, 2021. The copyright holder for this preprint (which was not certified by peer review) is the author/funder. All rights reserved. No reuse allowed without permission.



744

745

746 **Extended Data Fig. 3. Ectopic expression of INO80 rescues the nascent mRNA synthesis**

747 **defect of *ino80Δ* cells.**

748 **a,** Scatterplot analysis for fold changes in newly synthesized mRNA between *ino80Δ* cells

749 expressing a WT allele of *INO80* from the pRS416 plasmid (*pINO80*) and WT cells

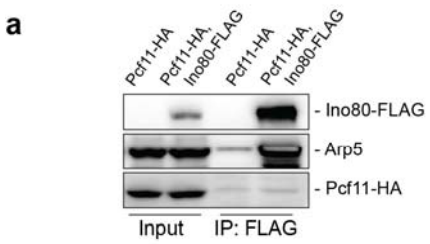
750 transformed with the empty vector pRS416 (EV) plotted on a $\log_2$ scale. Analysis as in

751 Fig.3a. **b,** Fold changes in mRNA decay rates between *ino80Δ* and WT for the indicated

752 genes as calculated by cDTA analysis. **c,** RT-qPCR analysis for *HPT1* RNA was conducted

753 in WT and *ino80Δ* before (T_0) and after addition of thiolutin in YPD as in Fig. 3d.

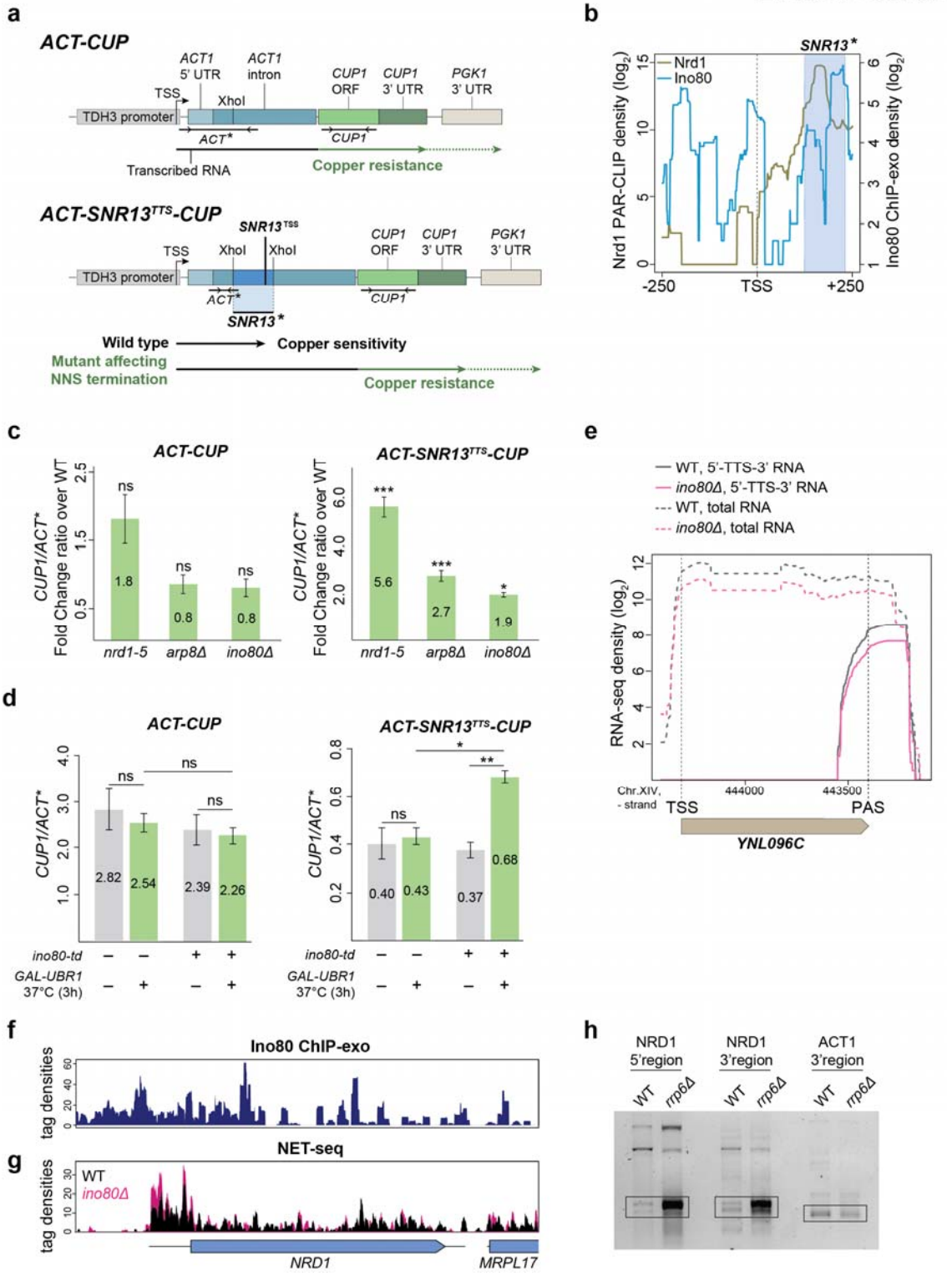
bioRxiv preprint doi: https://doi.org/10.1101/2020.03.02.973685; this version posted October 14, 2021. The copyright holder for this preprint (which was not certified by peer review) is the author/funder. All rights reserved. No reuse allowed without permission.



Extended Data Fig. 4. INO80 does not interact with Pcf11.

a, Nucleic acid-free lysates from cells co-expressing Pcf11-HA with Ino80 either untagged or tagged with FLAG epitope were subjected to FLAG-IP. Inputs and IP samples were immunoblotted for FLAG, Arp5 and HA. Samples were resolved in the same SDS-page gel.

bioRxiv preprint doi: https://doi.org/10.1101/2020.03.02.973685; this version posted October 14, 2021. The copyright holder for this preprint (which was not certified by peer review) is the author/funder. All rights reserved. No reuse allowed without permission.



bioRxiv preprint doi: https://doi.org/10.1101/2020.03.02.973685; this version posted October 14, 2021. The copyright holder for this preprint (which was not certified by peer review) is the author/funder. All rights reserved. No reuse allowed without permission.

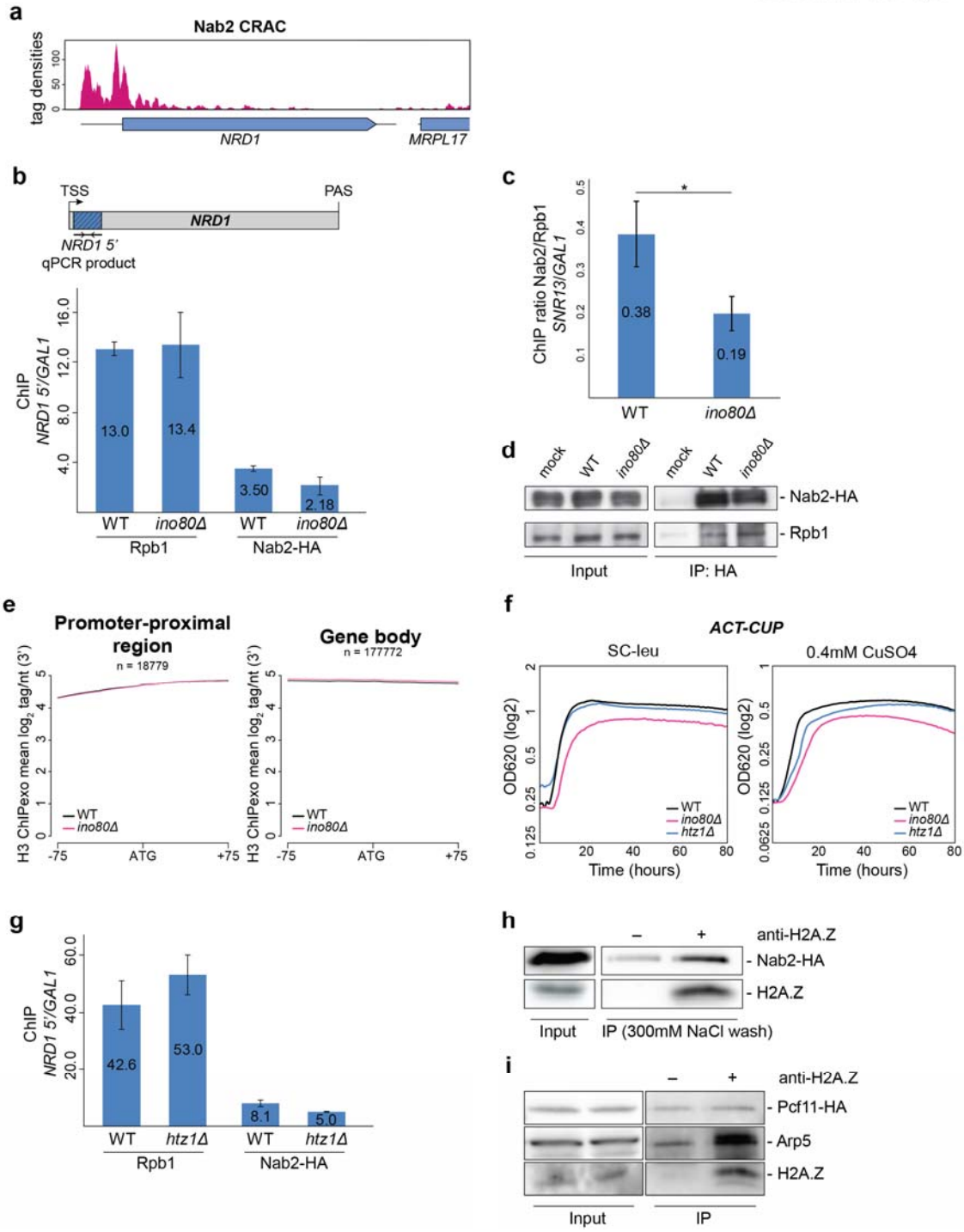
Extended Data Fig. 5. Defective NNS-dependent transcription termination in *ino80Δ* cells.

a, Schematic representation of the *ACT-CUP* (pGAC24) and *ACT-SNR^{TTS}-CUP* (pGAC24-SNR13^{TTS}) reporter systems for transcription termination reported in[8]. The regions amplified by RT-qPCR for *ACT** and *CUP1* are underlined. The region of the *SNR13* gene between +125 to +232bp from TSS that was cloned in the *ACT-SNR13^{TTS}-CUP* plasmid[8] is shaded in blue (*SNR13**). The expected phenotype of cells transformed with either the *ACT-CUP* or the *ACT-SNR13^{TTS}-CUP* plasmid is shown. **b,** Snapshot of Nrd1 PAR-CLIP density profile from[81] and Ino80 ChIP-exo density profile from [33] across the *SNR13* snoRNA gene. Tags were aligned relative to TSS and plotted on a $\log_2$ scale. The region between +125 to +232bp from TSS cloned in the *ACT-SNR13^{TTS}-CUP* plasmid described in (a)[8] is highlighted in blue (*SNR13**). **c,** RT-qPCR analysis for the *CUP1*/*ACT** ratio was conducted in the indicated strains transformed with either the *ACT-CUP* (left panel) or *ACT-SNR^{TTS}-CUP* (right panel) plasmids. Bars, standard errors from three independent experiments. Asterisks indicate statistical significance of the change in the respective mutant compared to the WT as calculated by t-test. ns: non-significant. *, $p<0.05$. ***, $p<0.001$. **d,** RT-qPCR analysis was conducted in both WT and the *ino80-td* degron-inducible strain (*ino80-td*) [82] transformed with the *ACT-CUP* control plasmid described in a. Galactose-induced activation for 3 hours at 37^{o}C (+) and glucose-induced suppression (–) of the *UBR1* N-recognin in the two strains is indicated. Bars, standard errors from four independent experiments. p-values were calculated by t-test after testing for normal distribution by Shapiro-Wilk test. ns, non-significant. **e,** Snapshot representing RNA-seq densities in WT and *ino80Δ* across the ribosomal protein coding gene YNL096C. Solid lines, density of reads encompassing the transcription termination site (5'-TTS-3') as described in Fig. 6c. Analysis was performed around the polyadenylation site (PAS). Broken lines, total RNA-seq density. Genomic coordinates of

bioRxiv preprint doi: https://doi.org/10.1101/2020.03.02.973685; this version posted October 14, 2021. The copyright holder for this preprint (which was not certified by peer review) is the author/funder. All rights reserved. No reuse allowed without permission.

786 Chromosome XVI around the *YNL096C* gene are shown. The closest gene downstream of
787 *YNL096C* is the *PHO23* mRNA gene (TSS: Chromosome XIV, 442509). **f,** Snapshot
788 representing ChIP-exo densities of Ino80 from [41] across the *NRD1* gene. **g,** Snapshot
789 representing NET-seq densities in WT and *ino80Δ* across the *NRD1* gene. **h,** Representative
790 image of nested 3'RACE analysis of termination events at the *NRD1* 5' and 3' regions
791 according to the scheme in Figure 6e and at the 3' of *ACT1* gene in WT and *rrp6Δ* on an
792 agarose gel. Boxes indicate the most frequent termination sites. Ladder is 100bp. *ACT1*
793 serves as loading control.

bioRxiv preprint doi: https://doi.org/10.1101/2020.03.02.973685; this version posted October 14, 2021. The copyright holder for this preprint (which was not certified by peer review) is the author/funder. All rights reserved. No reuse allowed without permission.



Extended Data Fig. 6. Co-transcriptional recruitment of Nab2 to chromatin depends on INO80 and H2A.Z.

a, Snapshot representing CRAC densities for Nab2 from [4] across the *NRD1* gene. **b,** Chromatin immunoprecipitation for Rpb1 and Nab2-HA in WT and *ino80Δ* cells. Fold

bioRxiv preprint doi: https://doi.org/10.1101/2020.03.02.973685; this version posted October 14, 2021. The copyright holder for this preprint (which was not certified by peer review) is the author/funder. All rights reserved. No reuse allowed without permission.

799 enrichment analysis at the promoter-proximal region of *NRD1* gene (*NRD1 5'*) (upper panel,
800 shaded in dark blue) was conducted as Fig. 7a. **c,** Chromatin immunoprecipitation for Nab2-
801 HA and Rpb1 in WT and *ino80Δ* cells. Fold enrichment of each protein at the TTS region of
802 *SNR13* gene was calculated relative to the *GAL1* promoter after correction for input DNA
803 levels. ChIP ratio at the TTS region of *SNR13* gene was calculated as Fold enrichment of
804 Nab2-HA over Fold enrichment of Rpb1. Bars, standard errors from four independent
805 experiments. p-values were calculated by t-test after testing for normal distribution by
806 Shapiro-Wilk test. *, $p<0.05$. **d,** Nucleic acid-free lysates from WT and *ino80Δ* cells both
807 expressing Nab2-HA were subjected to HA-IP. Inputs and IP samples were immunoblotted
808 for Rpb1 and HA. Mock, WT protein lysate subjected to immunoprecipitation with a control
809 IgG antibody. **e,** Metagene analysis for ChIP-exo density profiles of histone H3 in WT and
810 *ino80Δ* aligned at the A nucleotide of the ATG sites in the TSS to TSS+200bp (Promoter-
811 proximal) and the TSS+200 to PAS (Gene body) regions. n=Number of ATG sites in each
812 region. **f,** Cell proliferation analysis for the indicated strains transformed with the *ACT-CUP*
813 plasmid grown exponentially in SC-ura (left panel) and in SC-ura liquid media containing
814 0.4mM $CuSO_4$ (6-AU) (right panel) for the indicated time. Cell density was measured at
815 OD^{620} and is shown on a $\log_2$ scale. **g,** Chromatin immunoprecipitation for Rpb1 and Nab2-
816 HA in WT and *htz1Δ* cells. Fold enrichment analysis at the promoter-proximal region of
817 *NRD1* gene (*NRD1 5'*) was conducted as Fig. 7a. **h,** Nucleic acid-free lysates from WT cells
818 expressing Nab2-HA were subjected to immunoprecipitation with either an anti-H2A.Z
819 antibody (+) or a non-specific IgG antibody as a control (–), then washed in the presence of
820 300mM NaCl. Inputs and IP samples were immunoblotted for HA and H2A.Z. All analysis
821 was conducted from the same SDS-page gel. **I,** Nucleic acid-free lysates from cells
822 expressing Pcf11-HA were subjected to immunoprecipitation with either an anti-H2A.Z
823 antibody (+) or a non-specific IgG antibody as a control (–). Inputs and IP samples were

bioRxiv preprint doi: https://doi.org/10.1101/2020.03.02.973685; this version posted October 14, 2021. The copyright holder for this preprint (which was not certified by peer review) is the author/funder. All rights reserved. No reuse allowed without permission.

824 immunoblotted for HA, Arp5 and H2A.Z. The western for Pcf11-HA was over-exposed in
825 order to detect the background levels of Pcf11 binding to the beads. All analysis was
826 conducted from the same SDS-page gel.
827

bioRxiv preprint doi: https://doi.org/10.1101/2020.03.02.973685; this version posted October 14, 2021. The copyright holder for this preprint (which was not certified by peer review) is the author/funder. All rights reserved. No reuse allowed without permission.

828 **Extended Data Table 1 - Yeast strains used in this study**

Name	Genotype	Source
YM50	LS20 [*MatΔ ade2 can1r cyh2r lys S URA3-52 trp1Δ his3-Δ200GAL:HO leu 2Δ*]	Sandell & Zakian, *Cell* 1993
YM85	LS20 *ino80Δ::KANMX*	Papamichos-Chronakis & Peterson, *Nat Struct Mol Biol* 2008
YM133	W303 *ubr1Δ::HIS3-GAL-Myc-UBR1*	Jónsson *et al.*, *Mol Cell* 2004
YM135	W303 *ubr1Δ::HIS3-GAL-Myc-UBR1 ino80Δ::URA3-HA-ino80-td*	Jónsson *et al.*, *Mol Cell* 2004
YM143	LS20 *htz1Δ::hisG-ura3Δ*	Papamichos-Chronakis *et al.*, *Cell* 2011
YM181	LS20 *arp8Δ::KANMX*	Papamichos-Chronakis *et al.*, *Cell* 2011
YM198	LS20 *hda1Δ::HPHMX*	This study
YM199	LS20 *arp8Δ::KANMX hda1Δ::HPHMX*	This study
YM311	W303 [*MATa ade2-1 can1-100 his3-11 leu2,3,112 trp1-1 ura3-1*]	Verma *et al.*, *Mol Cell* 2011
YM334	W303 *arp8Δ::KANMX*	Lafon *et al.*, *Mol Cell* 2015
YM467	LS20 *dst1Δ::KANMX*	This study
YM468	LS20 *rpb9Δ::KANMX*	This study
YM498	LS20 *rco1Δ::HPHMX*	This study
YM499	LS20 *arp8Δ::KANMX rco1Δ::HPHMX*	This study
YM753	BY4741 [*MATa his3Δ1 leu2Δ0 met15Δ0 ura3Δ0*] *NRD1-3XHA::HIS3*	This study
YM801	46a [*MATa ura3 his3 trp1 lys2 ade2 leu2 cup1Δ*]	Steinmetz & Brow, *Mol Cell Biol* 1996
YM802	46a *nrd1-5*	Steinmetz & Brow, *Mol Cell Biol* 1996
YM838	LS20 *arp5Δ::KANMX*	This study
YM850	BY4741 *PCF11-3XHA::HIS3*	This study
YM885	LS20 *RPB1-3XFLAG::KANMX*	This study

bioRxiv preprint doi: https://doi.org/10.1101/2020.03.02.973685; this version posted October 14, 2021. The copyright holder for this preprint (which was not certified by peer review) is the author/funder. All rights reserved. No reuse allowed without permission.

YM900	BY4741 *PCF11-3XHA::HIS3 INO80-5XFLAG::NATMX*	This study
YM901	BY4741 *NRD1-3XHA::HIS3 INO80-5XFLAG::NATMX*	This study
YM903	LS20 *RPB1-3XFLAG::KANMX ino80Δ::HPHMX*	This study
YM1002	46a *arp8Δ::HPHMX*	This study
YM1036	46a *nrd1-5 arp8Δ::HPHMX*	This study
YM1085	LS20 *xrn1Δ::KANMX*	This study
YM1139	LS20 *rrp6Δ::KANMX*	This study
YM1141	46a *rco1Δ::KANMX*	This study
YM1147	46a *nrd1-5 arp8Δ::HPHMX rco1Δ::KANMX*	This study
YM1197	BY4741 *abd1-DAmP::KANMX*	Breslow *et al*, *Nat Methods* 2008
YM1325	LS20 *NAB2-3XHA::KANMX*	This study
YM1331	LS20 *NAB2-3XHA::KANMX ino80Δ::HPHMX*	This study
YM1332	LS20 *NAB2-3XHA::KANMX ino80Δ::HPHMX*	This study
YM1452	LS20 *NAB2-3XHA::KANMX htz1Δ::HPHMX*	This study

829

bioRxiv preprint doi: https://doi.org/10.1101/2020.03.02.973685; this version posted October 14, 2021. The copyright holder for this preprint (which was not certified by peer review) is the author/funder. All rights reserved. No reuse allowed without permission.

Extended Data Table 2 – Expression of genes encoding for RNA surveillance proteins is similar in WT, *ino80Δ* and *arp8Δ* cells. RNA abundance for the listed genes was measured by spiked-in total RNA-seq analysis in the indicated strains. Values represent average from two biological replicates for each experiment. The RNA-seq experiment for WT[(1)] and *ino80Δ* was conducted independently from WT[(2)] and arp8*Δ*. Values represent average from two biological replicates for each experiment.

Pathway/complex	Gene	WT[(1)]	*ino80Δ*	Fold Change	WT[(2)]	*arp8Δ*	Fold Change
NNS	*NRD1*	0.61	0.67	**1.1**	0.43	0.37	**0.8**
	NAB3	0.54	0.44	**0.8**	0.30	0.30	**1.0**
	SEN1	0.46	0.58	**1.3**	0.29	0.25	**0.8**
Exosome	*RRP6*	0.68	0.54	**0.8**	0.46	0.46	**1.0**
	DIS3/RRP44	0.82	0.73	**0.9**	0.64	0.62	**1.0**
TRAMP	*MTR4*	0.97	0.74	**0.8**	0.87	0.89	**1.0**
	TRF4	0.45	0.48	**1.1**	0.28	0.32	**1.1**
	AIR1	0.38	0.30	**0.8**	0.29	0.29	**1.0**
	AIR2	0.21	0.22	**1.1**	0.11	0.15	**1.4**
Cleavage and Polyadenylation	*HRP1*	1.21	1.01	**0.8**	1.04	0.83	**0.8**
	PCF11	0.26	0.24	**0.9**	0.19	0.18	**1.0**
	NAB2	0.70	0.59	**0.8**	0.51	0.54	**1.1**
	PAB1	8.95	6.85	**0.8**	4.53	3.89	**0.9**
Capping	*CEG1*	0.42	0.44	**1.1**	0.19	0.22	**1.1**
	CET1	0.27	0.26	**1.0**	0.17	0.19	**1.1**
Early mRNA processing	*CBC1*	0.96	0.74	**0.8**	0.58	0.68	**1.2**
	GBP2	1.43	1.09	**0.8**	0.83	0.74	**0.9**
	THO2	0.48	0.51	**1.0**	0.27	0.31	**1.2**
Export	*MEX67*	0.52	0.50	**1.0**	0.32	0.34	**1.1**
Cytoplasmic decay	*XRN1*	1.87	1.76	**0.9**	0.91	0.91	**1.0**
	SKI2	0.40	0.40	**1.0**	0.28	0.31	**1.1**

bioRxiv preprint doi: https://doi.org/10.1101/2020.03.02.973685; this version posted October 14, 2021. The copyright holder for this preprint (which was not certified by peer review) is the author/funder. All rights reserved. No reuse allowed without permission.

Extended Data Table 3 – Readthrough index (RI) of budding yeast *SNR* snoRNA genes as measured by total RNA-seq from the indicated strains. The RNA-seq experiment for WT[(1)] and *ino80Δ* was conducted independently from WT[(2)], *xrn1Δ*, *rrp6Δ*. Values represent average from two biological replicates for each experiment.

	WT[(1)]	***ino80Δ***	**WT[(2)]**	***xrn1Δ***	***rrp6Δ***
NME1	0.05	0.10	0.09	0.12	0.06
SNR11	0.18	0.17	0.26	0.23	0.24
SNR128	0.29	0.36	0.36	0.38	0.29
SNR13	0.15	0.28	0.44	0.36	0.25
SNR161	0.20	0.21	0.30	0.20	0.15
SNR189	0.22	0.23	0.47	0.39	0.33
SNR190	0.01	0.01	0.01	0.01	0.01
SNR3	0.90	1.05	0.91	0.87	0.68
SNR30	0.11	0.16	0.25	0.24	0.51
SNR31	0.18	0.15	0.17	0.17	0.13
SNR32	0.64	0.63	0.73	0.83	0.67
SNR33	0.41	0.39	0.47	0.37	0.51
SNR34	0.49	0.55	0.55	0.41	0.29
SNR35	0.17	0.20	0.27	0.17	0.17
SNR36	0.36	0.38	0.33	0.29	0.25
SNR37	0.32	0.37	0.46	0.42	0.72
SNR39B	0.41	0.57	0.50	0.41	0.93
SNR4	0.17	0.18	0.18	0.15	0.34
SNR40	0.61	0.70	0.62	0.70	0.53
SNR41	0.23	0.22	0.22	0.31	0.34
SNR42	0.42	0.37	0.98	0.59	0.95
SNR43	0.23	0.24	0.35	0.40	0.73
SNR45	1.15	1.04	0.99	0.84	1.57
SNR46	0.37	0.58	0.52	1.06	0.20
SNR47	0.56	1.21	0.52	0.56	1.61
SNR48	0.59	0.71	0.75	0.76	0.93
SNR49	0.53	0.62	0.43	0.41	0.21
SNR5	0.42	0.44	0.53	0.45	0.57
SNR50	1.30	1.08	1.00	0.97	1.76
SNR51	0.79	1.30	1.03	0.76	1.45
SNR52	0.47	0.51	0.52	0.42	0.60
SNR53	0.54	0.79	0.52	0.65	0.74
SNR55	0.39	0.57	0.42	0.55	0.28
SNR56	0.40	0.68	0.46	0.52	2.72
SNR57	0.66	0.64	0.60	0.62	0.71
SNR58	1.01	0.87	1.14	0.69	1.07

bioRxiv preprint doi: https://doi.org/10.1101/2020.03.02.973685; this version posted October 14, 2021. The copyright holder for this preprint (which was not certified by peer review) is the author/funder. All rights reserved. No reuse allowed without permission.

SNR61	1.57	2.83	1.19	0.85	2.76
SNR62	1.78	2.03	1.66	1.51	3.55
SNR63	0.40	0.52	0.66	0.43	0.55
SNR64	0.33	0.49	0.22	0.23	0.49
SNR65	0.74	0.95	1.09	0.30	3.17
SNR66	1.23	2.42	1.07	1.33	1.74
SNR67	1.07	1.01	1.08	1.14	1.44
SNR68	0.36	0.75	0.82	0.60	1.09
SNR69	0.68	0.88	0.75	0.80	0.70
SNR70	1.56	1.72	2.16	2.34	1.28
SNR71	1.38	2.61	1.41	1.39	3.46
SNR72	0.39	0.62	0.33	0.37	0.42
SNR74	1.10	1.29	1.05	1.53	0.47
SNR75	2.10	2.46	1.72	2.14	1.37
SNR76	0.57	0.52	0.46	0.44	0.30
SNR77	1.07	1.27	1.07	1.13	0.62
SNR78	3.67	4.40	4.26	5.35	4.26
SNR79	1.73	1.63	1.65	1.23	2.45
SNR8	0.27	0.27	0.21	0.22	0.27
SNR80	0.06	0.17	0.14	0.13	0.23
SNR81	0.15	0.28	0.23	0.19	0.12
SNR82	0.66	0.77	0.92	0.89	0.94
SNR83	0.35	0.46	0.46	0.30	1.03
SNR84	0.58	0.77	0.60	0.81	0.26
SNR85	0.02	0.02	0.03	0.02	0.08
SNR86	0.41	0.40	0.25	0.26	0.17
SNR87	0.93	1.16	1.04	0.90	1.38
SNR9	0.28	0.32	0.38	0.36	0.27

841

bioRxiv preprint doi: https://doi.org/10.1101/2020.03.02.973685; this version posted October 14, 2021. The copyright holder for this preprint (which was not certified by peer review) is the author/funder. All rights reserved. No reuse allowed without permission.

METHODS

Bioinformatics Tools and genome annotations

Unless otherwise indicated, version of the tools used for all bioinformatics analyses are as follows:

Samtools version 1.10

Bedtools version 2.29.2

Bowtie2 version 2.4.1

Hisat2 version 2.2.0

R version 3.6.2

BamCoverage version 3.5.0

Fastqc version 0.11.9

Cutadapt version 2.10

Trim_galore 0.6.4

MarkDuplicates version 2.23.1

FeatureCounts version 2.0.0

The *Saccharomyces cerevisiae* reference genome (S288C version R64-2-1) was downloaded from Saccharomyces Genome Database (https://www.yeastgenome.org/). The annotation used in the analysis for mRNA genes was produced by Antonin Morillon's lab, and based on CAGE-seq. This also includes the following annotations: XUT genes from [83], SUT and CUT genes from XUT et al (2009) and NUT genes from [16]. Annotations for other transcript types (snRNA, snoRNA, etc) were downloaded from Saccharomyces Genome Database.

The *Schizosaccharomyces pombe* reference genome and annotation (ASM294v2.47) were downloaded from pombase (www.pombase.org). Only protein coding genes were used in this analysis.

NET-seq analyses

bioRxiv preprint doi: https://doi.org/10.1101/2020.03.02.973685; this version posted October 14, 2021. The copyright holder for this preprint (which was not certified by peer review) is the author/funder. All rights reserved. No reuse allowed without permission.

867 NET-seq was performed from yeast strains containing Rpb1-FLAG (3XFLAG), alone or
868 along with deletion of *INO80*. All strains appeared fully functional, with identical Ser2 and
869 Ser5 phosphorylation levels on Rpb1 C-terminal domain and identical growth rates to the
870 respective untagged strains (data not shown). NET-Seq libraries were constructed from
871 biological duplicates of YM903 (*ino80Δ*, *RPB1-FLAG*) and YM885 (WT, *RPB1-FLAG*) cells
872 and sequenced as previously described[84]. Reads shorter than 10 nt were filtered out. Reads
873 were mapped with Bowtie2 using default parameters. Duplicates reads were marked using
874 Picard MarkDuplicates. Coverage files (bigWig) were produced by custom script. Reads
875 locations from the alignment files (bam) were turned into bed files using bedtools bamtobed
876 (with « -split » option), ignoring duplicates reads and reads with mapping quality below 30,
877 piled up along the genome and turned into bigWig files using a python script. FeatureCounts
878 was used for quantification with options « -O --fraction s 2 --ignoreDup ». Normalization
879 factors were computed using DESeq2 method, using the whole count matrix. Travelling
880 Ratio was computed as: (read density on gene body) / (read density on TSS), with gene body
881 the region between TSS+200 nt to TTS and TSS the region from TSS to TSS + 200 nt. Read
882 density was computed as : (# reads on region / region length) *1000.

883 **4tU labeling and purification of newly synthesized RNAs**

884 RNA labeling and purification were performed as previously described with some minor
885 adjustments[45,85]. Briefly, 20 mL of wildtype and mutant S. cerevisiae cells were grown at
886 30°C to an OD600 ≈0.8 in YPD. Newly synthesized (ns) RNAs were labelled for 6 min with
887 4-thiouracil (4tU, Sigma-Aldrich) added to the yeast cultures to a final concentration of 5
888 mM. Similarly, S. pombe RNAs were labeled for 6 min in YES medium at 32°C. Cells were
889 pelleted directly after labeling and flash frozen in liquid nitrogen. All experiments were
890 performed in biological triplicates. Prior to RNA extraction S. cerevisiae and S. pombe cells
891 were mixed in a ratio of 3:1 and total RNA was extracted with Ribopure Yeast Kit (Ambion,

bioRxiv preprint doi: https://doi.org/10.1101/2020.03.02.973685; this version posted October 14, 2021. The copyright holder for this preprint (which was not certified by peer review) is the author/funder. All rights reserved. No reuse allowed without permission.

892 Life Technologies) according to the manufacturer's guidelines. 150 µg of total RNA were
893 biotinylated for 3 hours at room temperature using 200 µL of 1 mg/mL EZ-link HPDP-
894 Biotin (Pierce) with 100 µL of biotinylation buffer (100 mM Tris- HCl pH 7.5, 10 mM
895 EDTA) and 100 µL of DMSO adjusted to a final volume of 1 mL with DEPC-treated RNase-
896 free water (Sigma-Aldrich). After biotinylation, excess biotin was removed by mixing 1 mL
897 of chloroform to the reaction and the liquid phases were separated by centrifugation for 5 min
898 at 4°C and max speed. The aqueous phase was recovered and precipitated with isopropanol
899 (1/10 volumes 5M NaCl and 2.5 volumes isopropanol). The recovered RNA was resuspended
900 in 100 µL DEPC-treated RNase-free water and incubated for 10 min at 65°C followed by 5
901 min on ice. nsRNAs were bound to 100 µL of µMACS streptavidin microbeads (Miltenyi
902 Biotec) for 90 min at room temperature and purification was performed using the µMACS
903 streptavidin starting kit (Miltenyi Biotec). Columns were first equilibrated with 1 mL of
904 washing buffer (100 mM Tris-HCl at pH 7.5, 10 mM EDTA, 1M NaCl, 0.1% Tween20).
905 Samples were loaded and the flow-through was reapplied 2 times to the columns. The
906 columns were washed five times with increasing volumes of washing buffer (600, 700, 800,
907 900, and 1000 µL). Ultimately, labeled RNAs were eluted twice with 200 µL of 100mM
908 DTT. nsRNAs were precipitated overnight in 1/10 volume of 3 M NaOAc, 3 volumes of
909 100% ethanol and 20 µg of RNA-grade glycogen. The RNAs were recovered by
910 centrifugation and RNA pellets were wash with ice-cold 70% ethanol and resuspended in 20
911 µL of DEPC-treated RNase-free water (Sigma-Aldrich). Samples were stored at −80°C until
912 further use. Differential gene expression analysis was performed using DESeq2 1.16.1
913 Bioconductor R package on Saccharomyces cerevisiae counts normalized with size factors
914 computed by the median-of-ratios method proposed by Anders and Huber on
915 Schizosaccharomyces pombe counts (Anders and Huber 2010). cDTA analysis was
916 performed as described (Schwalb et al. 2012).

bioRxiv preprint doi: https://doi.org/10.1101/2020.03.02.973685; this version posted October 14, 2021. The copyright holder for this preprint (which was not certified by peer review) is the author/funder. All rights reserved. No reuse allowed without permission.

917

918 **Total RNA-seq**

919 Yeast strains were processed in duplicate. ERCC RNA Spike-in control mixes (Ambion,
920 catalogue #4456740) were added to 1µg of total RNA according to manufacturer. Ribosomal
921 RNAs were depleted from total RNA using the RiboMinus™ Eukaryote v2 Kit (Life
922 Technologies). Depletion efficiency and quality control of rRNA-depleted RNA was assessed
923 by analysis in RNA Pico 6000 chip for 2100 Bioanalyzer (Agilent). Total RNA-seq libraries
924 were prepared from 50ng of rRNA-depleted RNA using the TruSeq® Stranded Total RNA
925 Sample Preparation Kit (Illumina). Paired-end sequencing (2x50 nt) was performed on a
926 HiSeq 2500 sequencer giving between 65 and 84 million reads. Reads were mapped using
927 version 2.0.6 of TopHat, with a tolerance of 3 mismatches and a maximum size for introns
928 2Kb. Tags densities were normalized on spike-in controls for all subsequent analyses.

929 **ChIP-exo**

930 The ChIP-exo assay has been previously described (Rhee HS, Pugh BF. ChIP-exo method for
931 identifying genomic location of DNA-binding proteins with near-single-nucleotide accuracy.
932 Curr Protoc Mol Biol. 2012;Chapter 21:Unit 21). In brief, yeast strains were grown to
933 exponential phase in yeast extract peptone (YP) + 2% dextrose (30°C to OD600 nm = 0.8),
934 then subjected to 1% formaldehyde crosslinking for 15 min at 25 °C. After quenched with
935 125mM final concentration of glycine for 5 min, cells were harvested and washed. Sonicated
936 chromatin was prepared by standard methods. Standard ChIP methods were used for histone
937 H3 (antibody Ab1791, Abcam) followed by lambda exonuclease treatment and library
938 construction. Libraries were sequenced on an Illumina 2000 sequencer. Reads were uniquely
939 mapped to the reference genome (sacCer3 build) using version 2.1.0 of Bowtie2 with a
940 tolerance of 1 mismatch in seed alignment. Data were normalized on the total number of
941 uniquely mapped reads, for each sample.

bioRxiv preprint doi: https://doi.org/10.1101/2020.03.02.973685; this version posted October 14, 2021. The copyright holder for this preprint (which was not certified by peer review) is the author/funder. All rights reserved. No reuse allowed without permission.

Cell proliferation analysis in liquid media

Liquid growth rate analysis was conducted using the CG-12 robot (S&P Robotics Inc.). Yeast cells transformed with a URA3-containing plasmid (pRS416) and grown exponentially in SC-ura at 30°C were diluted to OD620 0.1 in either SC-ura or SC-ura + 50µg/ml 6-AU and four 150µl samples from each strain were plated onto 96-well transparent plates covered with breathable films. Plates were incubated at 30°C for several days and OD620 was measured in the CG-12 robot (S&P Robotics Inc.) every hour with a shaking of 1000rpm for 1 minute before each read. Liquid growth rate analysis was not possible in the *nrd1-5* and associated strains due to flocculation. All cell proliferation experiments were repeated at least twice.

Growth rates analysis on agar plates

Growth of yeast strains was compared by plating 5-fold serial dilutions on SC / SC-inositol, SC-ura / SC-ura + 50µg/ml 6-azauracil (6-AU, Sigma), SC-leu / SC-leu + 0.4mM CuSO4 (Sigma) or SC-leu / SC-leu + 0.25 CuSO4 and incubating the plates at 30°C for several days. All plating experiments were performed at least three times.

RT-qPCR

Total RNA was extracted either with RNeasy Mini Kit (Qiagen) or by classical acid phenol-chloroform extraction. RNAs abundance was measured with SuperScript® III Platinum® SYBR® Green One-Step qRT-PCR Kit (Invitrogen) using specific primers for the targets of interest in a 10µl reaction volume, on Applied Biosystem Step-One Plus machines. RNAs abundance of each sample was compared with standard curves analysis. Abundance of *CUP1* from transcriptional read-through analyses using the *ACT-CUP* reporter system was compared to *ACT** RNA specifically transcribed from the same plasmid (Extended Data Fig.5a). Abundance of *NRD1* promoter-proximal RNA (*NRD1* 5') was compared to levels of *NRD1* promoter-distal RNA (*NRD1* 3').

Co-immunoprecipitation

bioRxiv preprint doi: https://doi.org/10.1101/2020.03.02.973685; this version posted October 14, 2021. The copyright holder for this preprint (which was not certified by peer review) is the author/funder. All rights reserved. No reuse allowed without permission.

Benzonase-treated yeast cell extracts were incubated with 20µl Anti-FLAG Affinity Gel (Sigma Aldrich) in 10mM Tris-Cl pH 7.5, 150mM NaCl, 0.05mM EDTA, 0.5% NP40, 1X Protease Inhibitor Cocktail (Roche) and 0.01mM PMSF for 3h. Beads were washed twice in 10mM Tris-Cl pH 7.5, 150mM NaCl, 0.05mM EDTA, 1X Protease Inhibitor Cocktail (Roche) and 0.01mM PMSF and resuspended in SDS sample buffer. Western blot analyses were performed using Monoclonal anti-FLAG M2 antibody (Sigma F3165), Anti-HA tag antibody (Abcam, ab9110) and Anti-Arp5 antibody (Abcam, 12099). Images were acquired using Syngene G:BOX. The experiment was reproduced three times. Immunoprecipitations for H2A.Z and HA-tag were performed similarly on benzonase-treated yeast cell extract using 36µl Protein-A sepharose beads coupled with 6µl of appropriate antibody (Anti-H2A.Z, Active Motif 39647; Anti-HA tag, Abcam ab9110). Control immunoprecipitations (mock) were performed with a non-specific antibody (Anti-Rabbit IgG, Promega). Western blot analyses were performed using the following antibodies: Anti-HA, Anti-Arp5, Anti-H2A.Z and Anti-Rpb1 y-80 (Santa Cruz Biotechnology, sc-25758). After the immunoprecipitation for H2A.Z shown in Figure S6G, beads were washed twice in 10mM Tris-Cl pH 7.5, 150mM NaCl, 0.05mM EDTA, 1X Protease Inhibitor Cocktail (Roche) and 0.01mM PMSF, then washed a third time in the same buffer containing 300mM NaCl and finally resuspended in SDS sample buffer All experiments were reproduced three times.

Ino80 inducible degradation

The assay for inducible degradation of Ino80[82] was performed as previously described[35,86] Briefly, a degron tag was fused to INO80 (Ino80-td) in cells carrying the UBR1 gene, that encodes for the N-recognin Ubr1, under the control of the GAL1 promoter, and cells were transformed with the *ACT-CUP* plasmid reporter system (Extended Data Fig. 5a). Cells were grown in SC-leu media containing raffinose as carbon source at 25°C until OD600~0.6-0.7, then shifted to SC-leu media containing galactose to induce *UBR1* expression. Subsequently,

bioRxiv preprint doi: https://doi.org/10.1101/2020.03.02.973685; this version posted October 14, 2021. The copyright holder for this preprint (which was not certified by peer review) is the author/funder. All rights reserved. No reuse allowed without permission.

complete Ino80-td protein degradation by the Ubr1 pathway was induced by 3 hours of heat shock at 37°C. Cells were then immediately harvested by centrifugation at 4°C, 3500rpm for 3 minutes, then washed twice with ice-cold water and snap-frozen in liquid nitrogen for RNA analysis. Yeast cells carrying the GAL1-driven UBR1 gene along with an unmodified INO80 genes were use as control. Furthermore, both (GAL1-UBR1) and (GAL1-UBR1 Ino80-td) cells were grown in SC-leu media containing glucose as a negative control for UBR1 expression (Extended Data Fig. 5d, grey bars). RNA analysis was conducted by RT-qPCR as described above.

ChIP-qPCR

Chromatin immunoprecipitation was performed as previously described in (Papamichos-Chronakis M, Watanabe S, Rando OJ, Peterson CL. Global regulation of H2A.Z localization by the INO80 chromatin-remodeling enzyme is essential for genome integrity. Cell. 2011;144(2):200-13.). Sonication was performed on a Bioruptor® Pico sonication device (Diagenode) with ten 30-sec pulses with a 30-sec break between pulses. Immunoprecipitation was carried out with Anti-HA tag antibody (Abcam ab9110) and Anti-Rpb1 y-80 antibody (Santa Cruz Biotechnology, sc-25758) in parallel. The recovered DNA was subjected to quantitative real-time PCR using Platinum® SYBR® Green qPCR SuperMix-UDG Kit (Invitrogen) with specific primers for the targets of interest in 10µl reaction volume, on Applied Biosystem Step-One Plus machines.

RNA-IP

RNA immunoprecipitation was performed as described in (Selth LA, Gilbert C, Svejstrup JQ. RNA immunoprecipitation to determine RNA-protein associations in vivo. Cold Spring Harb Protoc. 2009;2009(6):pdb prot5234.). Sonication was performed on a Bioruptor® Plus sonication device (Diagenode) with two 15-sec pulses at 50% amplitude with a 1-min break

bioRxiv preprint doi: https://doi.org/10.1101/2020.03.02.973685; this version posted October 14, 2021. The copyright holder for this preprint (which was not certified by peer review) is the author/funder. All rights reserved. No reuse allowed without permission.

between pulses. Immunoprecipitation was carried out with Anti-HA tag antibody (Abcam ab9110). The recovered RNA was analysed by RT-qPCR as described above.

De novo analysis of public ChIP-exo and CRAC data

NAB3 and POLII CRAC data were taken from GEO dataset GSE70191 and processed as described in [56]. NAB2 and MTR CRAC data were taken from GEO dataset GSE46742 and processed as described in [4]. ChIP-exo H3 data were downloaded from NCBI SRA dataset SRA059355 and processed as described in [87].